Lifespan Trajectories of Asymmetry in White Matter Tracts

Praitayini Kanakaraj[1†], Sam Bogdanov[2†*], Michael E. Kim[1], Jessica Samir[3], Chenyu Gao[4], Karthik Ramadass[1,4], Gaurav Rudravaram[4], Nancy R. Newlin[1], Derek Archer[5,6,7], Timothy J. Hohman[5,6], Angela L. Jefferson[5,8,9,10,11], Victoria L. Morgan[12,13,14], Alexandra Roche[13], Dario J. Englot[1,4,12,14,15], Susan M. Resnick[16], Lori L. Beason Held[16], Laurie Cutting[7,17], Laura A. Barquero[17], Micah A. D'Archangel[17], Tin Q. Nguyen[7,13,17], Kathryn L.Humphreys[10], Yanbin Niu[10], Sophia Vinci-Booher[10], Carissa J. Cascio[18], The HABS-HD Study Team[A], Alzheimer's Disease Neuroimaging Initiative[B], The BIOCARD Study Team[C], Zhiyuan Li[19], Simon N. Vandekar[20], Panpan Zhang[5,20], John C. Gore[12,13,14], Stephanie J. Forkel[21,22,23], Bennett A. Landman[1,4,7,9,10,11,12,13,14,20], Kurt G. Schilling[12]

† These authors contributed equally to this work.

1 Vanderbilt University, Department of Computer Science, Nashville, TN, USA

2 Vanderbilt University, Medical Scientist Training Program, Nashville, TN, USA

3 Department of Psychological Science and Neuroscience, Belmont University, Nashville, TN, USA

4 Vanderbilt University, Department of Electrical and Computer Engineering, Nashville, TN, USA

5 Vanderbilt University Medical Center, Vanderbilt Memory and Alzheimer's Center, Nashville, TN, USA

6 Vanderbilt University Medical Center, Vanderbilt Genetics Institute, Nashville, TN, USA

7 Vanderbilt University, Vanderbilt Brain Institute, Nashville, TN, USA

8 Vanderbilt University Medical Center, Department of Medicine, Nashville, TN, USA

9 Vanderbilt University Medical Center, Department of Neurology, Nashville, TN, USA

10 Vanderbilt University, Department of Psychology and Human Development, Nashville, TN, USA

11 Vanderbilt University Medical Center, Department of Psychiatry and Behavioral Sciences, Nashville, TN, USA

12 Vanderbilt University Medical Center, Department of Radiology and Radiological Sciences, Nashville, TN, USA

13 Vanderbilt University Institute of Imaging Science, Nashville, TN, USA

14 Vanderbilt University, Department of Biomedical Engineering, Nashville, TN, USA

15 Vanderbilt University Medical Center, Department of Neurological Surgery, Nashville, TN, USA

16 Laboratory of Behavioral Neuroscience, National Institute on Aging, National Institutes of Health, Baltimore, MD, USA

17 Peabody College of Education and Human Development, Department of Special Education, Nashville, Tennessee, USA

18 University of Kansas, Life Span Institute and Department of Psychology, Lawrence, KS, USA

19 Department of Computer Science, Park University, Parkville, MO, USA

20 Vanderbilt University Medical Center, Department of Biostatistics, Nashville, TN, USA

21 Donders Centre for Cognition, Radboud University, Nijmegen, the Netherlands

22 Max Planck Institute for Psycholinguistics, Nijmegen, the Netherlands

23 Brain Connectivity and Behaviour Laboratory, Paris, France

A) HABS-HD MPIs and the HABS-HD Investigators

B) Data used in preparation of this article were obtained from the Alzheimer's Disease Neuroimaging Initiative (ADNI) database (adni.loni.usc.edu). As such, the investigators within the ADNI contributed to the design and implementation of ADNI and/or provided data but did not participate in analysis or writing of this report. A complete listing of ADNI investigators can be found at: http://adni.loni.usc.edu/wp-content/uploads/how_to_apply/ADNI_Acknowledgement_List.pdf

C) Data used in preparation of this article were derived from BIOCARD study, supported by grant U19 – AG033655 from the National Institute on Aging.

* Correspondence to: Sam Bogdanov

Vanderbilt University School of Medicine

2209 Garland Avenue, Nashville, TN 37240

samuel.b.bogdanov@vanderbilt.edu

Keywords: White Matter, Asymmetry, Diffusion MRI, Lateralization, Lifespan Development, Tractography

Abstract

Asymmetry in white matter is believed to give rise to the brain's capacity for specialized processing and is involved in the lateralization of various cognitive processes, such as language and visuo-spatial reasoning. Although studies of white matter asymmetry have been previously documented, they have often been constrained by limited age ranges, sample sizes, or the scope of the tracts and structural features examined. While normative lifespan charts for brain structures are emerging, comprehensive charts detailing white matter asymmetries across numerous pathways and diverse structural measures have been notably absent.

This study addresses this gap by leveraging a large-scale dataset of 26,199 typically developing and aging individuals, ranging from 0 to 100 years of age, from 42 primary neuroimaging studies. We generated comprehensive lifespan trajectories for 30 lateralized association and projection white matter tracts, examining 14 distinct microstructural and macrostructural features of these pathways.

Our findings reveal that: (1) asymmetries are widespread across the brain's white matter and are present in all 30 pathways; (2) for a given pathway, the degree and direction of asymmetry differ between features of tissue microstructure and pathway macrostructure; (3) asymmetries vary across and within pathway types (association and projection tracts); and (4) these asymmetries are not static, following unique trajectories across the lifespan, with distinct changes during development, and a general trend of becoming more asymmetric with increasing age (particularly in later adulthood) across pathways.

This study represents the most extensive characterization of white matter asymmetry across the lifespan to date, charting how lateralization patterns emerge, mature, and change throughout life. It provides a foundational resource for understanding the principles of white matter organization from early to late life, its relation to functional specialization and inter-individual variability, and offers a key reference for interpreting deviations during healthy development and aging as well as those associated with clinical populations.

Introduction

Brain asymmetry is an organizing principle of the nervous system that enables functional specialization.[1] Nearly two centuries ago, the pioneering clinical observations of Marc Dax (1836)[2,3] and later Paul Broca (1860s)[4,5] first linked left-hemisphere lesions to specific language deficits, establishing that complex cognitive functions are frequently lateralized to one hemisphere. This hemispheric division of labor is supported by an underlying structural architecture that enhances neural efficiency, allowing for parallel processing of different computations while minimizing cross-hemispheric conduction delays.[6] While asymmetries in functions as diverse as language,[7] visuospatial attention,[8] and motor control[9] are thought to depend on this lateralized brain circuitry, a comprehensive map of the anatomical scaffold (i.e., the white matter pathways) that supports these functions[10] across the human lifespan has yet to be charted.

The structural substrate of this functional specialization is the brain's white matter connectome.[11,12] Modern neuroimaging - specifically, diffusion-weighted MRI (dMRI) in combination with fiber tractography[13] - enables a noninvasive "virtual dissection" to segment and study the macrostructure of these pathways, as well as a "virtual histology" to probe their tissue microstructure.[14] Macrostructural measures describe morphometric features of pathways size and geometry including volume, lengths, and areas.[15] In contrast, microstructural measures are sensitive to cellular-level features including axonal coherence, packing density, and myelination.[16] Characterizing white matter asymmetry at both macro- and microstructure scales is essential, as they capture distinct biological properties that can follow different trajectories across development and aging.

Despite steady progress,[17-27] current knowledge of white-matter asymmetry rests largely on static snapshots from studies with modest sample sizes, narrow age ranges, and limited pathway and feature coverage. This has led to a fragmented literature in which the reported laterality for a given pathway often diverges, due to variations in sample size, age range/cohorts, and the specific structural feature(s) investigated. Moreover, most reports simply focus on testing whether the group mean differs from zero, rather than describing the age-specific distribution and how it changes across development and aging. This leaves unanswered questions about when asymmetry emerges, whether it strengthens or weakens at different life stages, and how widely it varies among healthy individuals at a given age. In short, the field lacks a lifespan-wide normative reference that quantifies the distribution of tract-level asymmetry across development and aging.

Here, we assemble 26,199 scans from 42 population-based cohorts spanning 0-100 years and construct age-varying brain asymmetry charts for white-matter pathways. Rather than centering on a binary test of whether asymmetry exists, we use an estimation framework to quantify the *magnitude*, *direction*, and *age-specific distribution* of asymmetry. Specifically, we: (1) establish normative lifespan trajectories for all investigated features and pathways; (2) identify which tracts and features exhibit asymmetry during key periods of development, young adulthood, and aging; (3) quantify the population-level distribution of right–left asymmetries within these periods; (4) determine whether - and at what ages - the direction of asymmetry reverses; and (5) assess how the magnitude of asymmetry changes dynamically (i.e., increases or decreases) across infancy, development, and later life. Together, these charts provide a population reference to contextualize individuals and cohorts, enabling future developmental and clinical studies to interpret asymmetry in an age-appropriate framework.

Materials and Methods

We analyzed 26,199 diffusion MRI scans from 42 population-based cohorts spanning 0-100 years (**Figure 1A**). For each participant, we derived tract-level measures for 30 bilateral white-matter pathways, capturing both microstructure (diffusion tensor imaging indices reflecting tissue organization, axonal density, and myelination) and macrostructure (tract volume, length, surface area) (**Figure 1B**). We computed a laterality index for every tract-feature pair (**Figure 1C**) and modelled age-varying centile curves to estimate the population distribution (i.e. typically showing 2.5th-25th-50th-75th-97.5th centiles) at each age. Our analyses summarized patterns across the developmental and aging windows, quantify inter-individual variability, and identify tracts and features with asymmetry or direction reversals.

We note that we emphasize and describe population *centiles* - which describe the expected range of individual values at a given age - rather than *confidence intervals*, which only quantify the precision of the median estimate; we therefore do not perform null-hypothesis significance tests, which are trivially positive at very large N. Study cohorts, image preprocessing, white matter pathway segmentation, statistical analysis and normative modeling are described below.

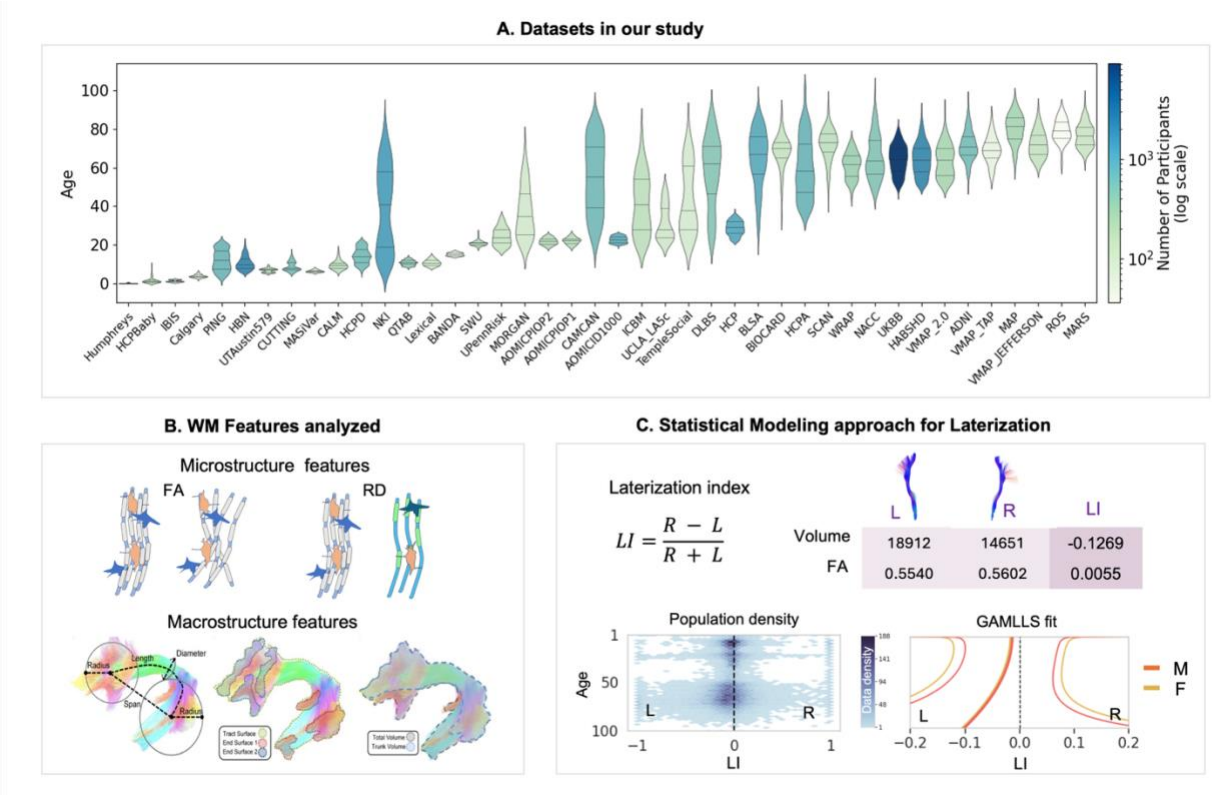

Figure 1. Overview of the study datasets, white matter features, and analytical framework. (**A**) Age distributions for each of the 42 contributing datasets (violin plots), illustrating broad coverage from 0–100 years. Color encodes the number of participants per dataset (log scale). (**B**) Features extracted for each of the 30 bilateral pathways. Microstructural indices (e.g., Fractional Anisotropy, and Mean, Axial and Radial diffusivities; FA, MD, AD, RD) summarize tissue organization and axonal/myelin density; macrostructural indices (e.g., tract volume, length, surface area) capture pathway size and geometry. (**C**) Analysis pipeline. For each participant, white matter pathways were segmented, and features were extracted. A Lateralization Index (LI) was calculated for each tract-feature pair. These LIs were used as input for a normative modeling framework (GAMLSS) to generate age-specific population centile curves.

Participants and Study Cohorts

The final dataset comprised 26,199 cross-sectional diffusion MRI scans aggregated from 42 independent, population-based cohorts (**Figure 1A**; see **Supplementary Table 1** for a detailed description of each cohort). To ensure a cross-sectional analysis, only the earliest available scan was included for any participant with longitudinal data, so that each individual is represented only once. The cohorts consist of typically developing and aging participants with broad geographic representation. Demographic information was harmonized across studies where available, including sex (44.4% female) and handedness (of 5,553 participants with handedness data, 10.6% were left-handed and 0.9% were ambidextrous). Cognitive and behavioral measures were not consistently available across the consortium and were therefore not included in the present analysis. All contributing studies received ethical approval from their local institutional review boards.

Diffusion MRI Processing Pipeline

All diffusion MRI data were processed with a single, standardized workflow using the PreQual pipeline (v 1.0.8) applied identically across cohorts to promote reproducibility.[28] This pipeline corrected for susceptibility-induced EPI distortions, head motion, and eddy current artifacts. To ensure consistency and reproducibility across the 42 cohorts, which varied in scanner and acquisition parameters, the same pipeline version was applied to all datasets, with specific flags adapted for each study's raw data structure. Following this preprocessing, diffusion tensor imaging (DTI) models were fitted to generate voxel-wise maps of fractional anisotropy (FA), mean diffusivity (MD), axial diffusivity (AD), and radial diffusivity (RD). Quality control was conducted at two stages.[29,30] First, automated logs and visual reports from PreQual were reviewed to identify corruption, gross motion, or failed corrections. Second, the derived scalar maps were visually inspected to verify anatomical plausibility and artifact mitigation. Scans failing QC at either stage were excluded prior to downstream analyses.

White Matter Pathway Segmentation and Feature Extraction

Tract Segmentation

The preprocessed dMRI data for each participant was upsampled to 1 mm isotropic resolution and input into TractSeg (v2.8),[31] a convolutional neural network (CNN) framework for white matter bundle segmentation.[31] TractSeg operates directly on local fiber orientation images, segmenting tracts without requiring whole-brain tractography or inter-subject registration. The pre-trained model automatically segmented 72 white matter bundle per participant. From these, we selected 60 lateral pathways (i.e., 30 bilateral tract pairs), excluding midline commissural structures, for asymmetry analyses. The set spans association and projection systems (with limbic, thalamic, and striatal subdivisions noted in **Table 1**).

Microstructural and Macrostructural Feature Definition

For each of the 30 segmented tract pairs, we computed two classes of features using the scilpy library (Sherbrooke Connectivity Imaging Lab's open-source toolkit, version 1.5.0)[32] (Figure **1B**).

Microstructural Features: We calculated four standard DTI indices that reflect cellular-level tissue properties.[16,33] To derive a single value for each tract, we computed a weighted average of the

metric across all voxels within the tract's mask, with the contribution of each voxel weighted by the number of streamlines passing through it.

- Fractional Anisotropy (FA): an index of directional coherence of diffusion, influenced by axonal organization/packing and myelin sheaths.
- Mean Diffusivity (MD): the average magnitude of water diffusion, sensitive to overall water mobility within tissue, influenced by axonal/myelin densities.
- Axial Diffusivity (AD): magnitude of water diffusion parallel to the principal fiber direction sensitive to the intra-axonal space and changes in axonal caliber and architecture.
- Radial Diffusivity (RD): magnitude of water diffusion perpendicular to the principal fiber direction. As myelin sheaths are a primary barrier to perpendicular diffusion, increased RD is often interpreted as reflecting demyelination or reduced axonal packing.

Macrostructural Features: We calculated three features describing the large-scale geometry and morphology of each tract[15,34]:

- Tract Volume: The total volume in mm^3 occupied by the pathway.
- Mean Streamline Length: The average length in mm of the streamlines constituting the tract, reflecting the trajectory extent.
- Tract Surface Area: The surface area in mm^2 of the geometric shape enclosing the tract, indexing bundle envelope size/complexity.

Table 1. List of 30 Bilateral White Matter Tracts Included in Asymmetry Analysis. As defined by the preset anatomical labels and segmentation outputs of the automated tractography tool TractSeg.

Pathways	Subcategory	Tract	Acronym
Association	Association	Arcuate Fasciculus	AF
		Middle Longitudinal Fasciculus	MLF
		Inferior Fronto-Occipital Fasciculus	IFO
		Inferior Longitudinal Fasciculus	ILF
		Superior Longitudinal Fasciculus I	SLF_I
		Superior Longitudinal Fasciculus II	SLF_II
		Superior Longitudinal Fasciculus III	SLF_III
	Limbic	Cingulum Bundle	CG
		Uncinate Fasciculus	UF
		Fornix	FX
Projection	Thalamic	Thalamo-prefrontal	T_PREF
		Thalamo-premotor	T_PREM
		Thalamo-precentral	T_PREC
		Thalamo-postcentral	T_POSTC
		Thalamo-parietal	T_PAR
		Thalamo-occipital	T_OCC
		Anterior Thalamic Radiation	ATR
	Striatal	Striato-fronto-orbital	ST_FO
		Striato-prefrontal	ST_PREF
		Striato-premotor	ST_PREM
		Striato-precentral	ST_PREC
		Striato-postcentral	ST_POSTC
		Striato-parietal	ST_PAR
		Striato-occipital	ST_OCC
	Projection	Corticospinal Tract	CST
		Frontal Pontine Tract	FPT
		Interior Cerebellar Peduncle	ICP
		Optic Radiation	OR
		Parieto-Occipital Pontine Tract	POPT
		Superior Cerebellar Peduncle	SCP

Statistical Analysis and Normative Modeling

Calculation of the Lateralization Index (LI)

For each micro- and macrostructural feature, we calculated a *Lateralization Index* (LI) to quantify the degree of asymmetry between the left (L) and right (R) hemispheres for each tract (**Figure 1C**). We used the formula $LI = \frac{R - L}{R + L}$. This index is bounded between -1 and 1. An LI of 0 indicates perfect symmetry. For this study, positive LI values indicate a rightward asymmetry (i.e., a higher value in the right-hemisphere tract), while negative LI values indicate a leftward asymmetry (a higher value in the left-hemisphere tract).[35]

Lifespan Normative Modeling Framework

We created lifespan charts of white matter asymmetry using a normative modeling approach. In the context of this large-scale dataset (N > 26,000), traditional null-hypothesis significance testing is not informative, as even biologically negligible asymmetries would yield a statistically significant result. Our goal was therefore not to ask the binary question of *whether* asymmetry exists, but rather to adopt an estimation framework to describe the full, age-specific distribution of the LI. This approach, analogous to the creation of pediatric growth charts,[36,37] allows for the characterization of the typical range of inter-individual variation at any given age.[38]

To model these complex, non-linear lifespan trajectories, we employed Generalized Additive Models for Location, Scale, and Shape (GAMLSS), implemented in R using the gamlss

package.[38,39] GAMLSS is highly suited for lifespan data as it flexibly models how the entire distribution of the LI - including its median (location, μ), variability (scale, σ), and shape - changes as a non-linear function of age.

For each of the 30 tracts and 7 features, a separate GAMLSS model was fit. We modeled the LI as a response variable following a normal distribution,[35] where both the mean (μ) and the standard deviation (σ) were modeled as functions of age, sex, and study cohort:

$$\mu = f_{\mu}(Age) + \beta_{\mu,sex} \,.\, Sex + u_{\mu,dataset} \quad (1)$$

$$\log(\sigma) = f_{\sigma}(Age) + \beta_{\sigma,sex} \,.\, Sex + u_{\sigma,dataset} \quad (2)$$

Here, $f_{\mu}(\cdot)$ and $f_{\sigma}(\cdot)$ are smooth functions of age, Sex is a fixed effect, and dataset random effects (u_{μ},u_{σ}) capture residual between-study variation. Allowing σ to vary with age accommodates age-dependent heteroscedasticity.

Age effects were represented with fractional polynomial (FP) smooths (order up to 2; powers drawn from [-2, −1, −0.5, 0, 0.5, 1, 2, 3], with logarithmic terms for repeated powers). For each tract–feature we fit candidate models with different FP choices for μ and σ and selected the specification with the lowest Bayesian Information Criterion (BIC).[40]

From the parameters of the best-fitting model, we generated smooth centile curves (e.g., 2.5th, 25th, 50th, 75th, and 97.5th percentiles) across a dense age grid, forming the final normative brain asymmetry charts (**Figure 1C**).

Characterizing Lifespan Dynamics

To examine white matter asymmetry across the lifespan, we used the normative LI trajectories derived from our GAMLSS models to address four core research questions:

1. What are the characteristics of exemplar lifespan asymmetry curves?

To answer this, we visualized the full, sex-specific centile curves (2.5th to 97.5th percentile) for selected white matter tracts and features to illustrate general patterns of development, aging, and inter-individual variability.

2. Which features and pathways exhibit population-level asymmetry at critical lifespan stages?

We summarized tract- and feature-specific asymmetries at four representative ages - 3, 12, 30, and 50 years - using heatmaps that display both the population median LI and the proportion of individuals with rightward vs. leftward lateralization.

3. Do asymmetries reverse direction across the lifespan?

We identified shifts in hemispheric dominance by assessing zero-crossings in the median LI trajectories, which indicate if and when the direction of population-level asymmetry changed (e.g., from leftward to rightward, or vice versa).

4. How does the magnitude of asymmetry evolve during different life stages?

To answer this, we quantified the rate of change in asymmetry within four distinct age windows: early/late childhood (2–12 years), adolescence (12–20 years), young adulthood (20–40 years), and middle/late adulthood (40–100 years). Within each window, we calculated the mean slope of the absolute value of the median LI curve to determine whether the *magnitude of asymmetry* was increasing (strengthening) or decreasing (attenuating) during that life stage.

Results

We constructed normative lifespan charts of white matter asymmetry by applying our statistical modeling framework to 26,199 individuals spanning 0-100 years. These charts characterize the magnitude, direction, and population-level variability for 7 micro- and macrostructural features across 30 bilateral white matter pathways. This comprehensive analysis revealed several key principles of brain lateralization, which are detailed in the following sections. We begin by illustrating the modeling approach and showing exemplar trajectories that highlight distinct patterns of development and aging.

What are the characteristics of exemplar lifespan asymmetry curves?

The normative lifespan charts revealed that white matter tracts exhibit highly heterogeneous and dynamic patterns of asymmetry, which varied substantially across different pathways, features, and ages. To orient the reader to these results, **Figure 2** illustrates the full centile-based lifespan trajectory for two features of the arcuate fasciculus (AF) – the FA and total volume. These charts depict the population median (50th percentile) and the spread of the population (from the 2.5th to the 97.5th percentile), with lateralization intuitively shown left-to-right along the x-axis, providing a comprehensive view of both the central tendency and the inter-individual variability in asymmetry at any given age.

Building on this, **Figure 3** displays a broader selection of exemplar trajectories for four well-studied pathways (AF, Anterior Thalamic Radiation [ATR], Frontal Pontine Tract [FPT], Corticospinal Tract [CST]) across six key micro- and macrostructural (FA, MD, AD, RD, tract volume, tract length) features. These charts highlight several overarching principles.

First, while asymmetry is common, its magnitude varies by feature type. Microstructural asymmetries were often subtle, with the bulk of the population having LI values between -0.05 and +0.05. For example, the AF showed a consistent leftward FA asymmetry with a population median LI ranging from -0.02 to -0.03 across age and $25^{th}/75^{th}$ centiles from -0.05 to -0.01. In contrast, macrostructural features exhibited a much wider range of individual variability, often spanning the range from -0.2 to +0.2, with larger median effects (e.g., median LI for ATR length ~0.05; FPT volume ~-0.07). Second, patterns were highly dependent on the combination of tract and metric, where pathways can show opposite lateralization directions across features, highlighting the need to study both micro- and macrostructure jointly. For example, the AF shows left-lateralization for FA and volume but right-lateralization for RD and length, or the ATR showing general leftward asymmetries for diffusivities and rightward volume and length asymmetries. Third, these asymmetries were not static but changed dynamically across the lifespan, with many tracts showing age-dependent increases or decreases in lateralization. Fourth, despite these complex dynamics, male and female median trajectories showed general overlap

across nearly all tracts and features, suggesting minimal sex differences in the average patterns of asymmetry. Finally, inter-individual variability was not constant, with wider centile bands in early childhood and older age suggesting a greater diversity of asymmetry patterns during these life stages.

All individual lifespan charts for all 30 tracts and 7 features are provided in the **Supplementary Material (Supplementary Fig. 2)**.

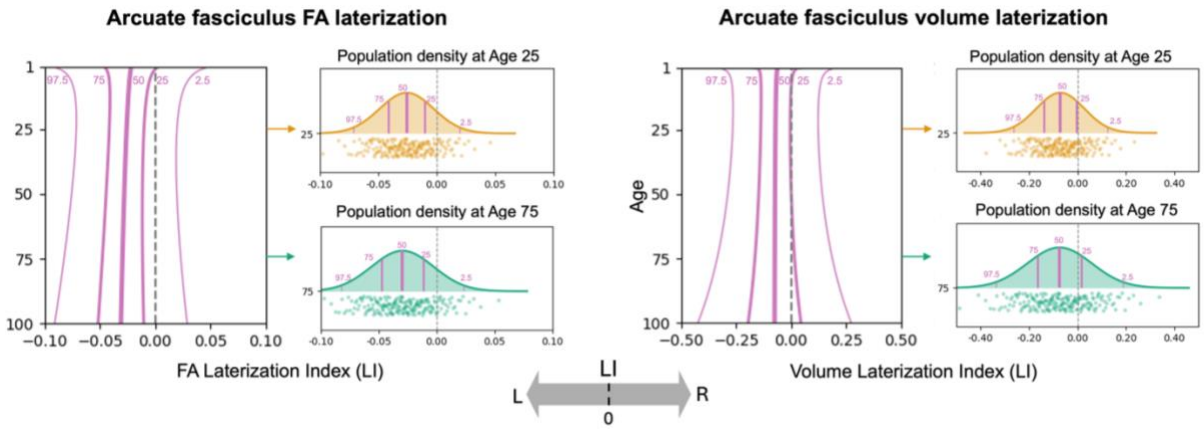

Figure 2. Exemplar asymmetry lifespan curves for the arcuate fasciculus (AF). Lifespan trajectories for fractional anisotropy (FA; a microstructural feature) and tract volume (a macrostructural feature) are shown. Lines represent the 2.5th, 25th, 50th (median), 75th, and 97.5th centile curves, illustrating the full population distribution of the Laterality Index (LI) across the lifespan. Negative values indicate leftward asymmetry, positive values indicate rightward asymmetry.

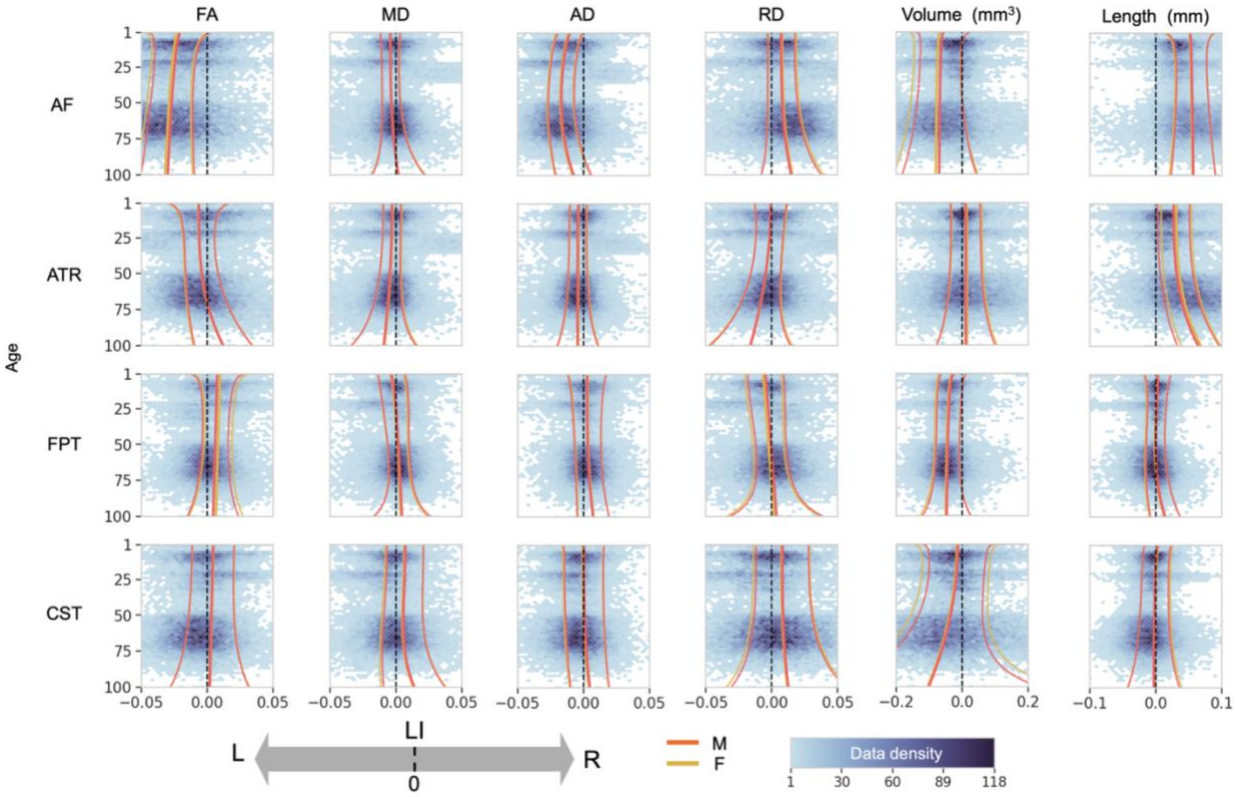

Figure 3. Diverse patterns of lifespan asymmetry across tracts and features. Lifespan trajectories of the LI are shown for four white matter tracts (arcuate fasciculus (AF), anterior thalamic radiation (ATR), frontal pontine tract (FPT), and corticospinal tract (CST)) and six features (FA, MD, AD, RD, volume, and length). Solid lines represent the population median (50th percentile), with the lighter bands showing the inter-quartile range (25th-75th percentiles). Red and yellow lines correspond to males and females, respectively. The plots highlight that the magnitude, direction, and age-related dynamics of asymmetry are highly specific to the tract and feature being measured. Full charts for all tracts and features are provided in **Supplementary Material (Supplementary Fig. S2)**.

Which features and pathways exhibit population-level asymmetry at critical lifespan stages?

To characterize asymmetry at discrete life stages, we examined the population median LI (**Figure 4**) and the percentage of individuals with rightward lateralization (**Figure 5**) at four key ages: 3, 12, 30, and 50 years. Together, the two figures convey both the typical direction/magnitude (median LI) and the population consensus (prevalence) for each tract–feature–age combination.

The results highlight a considerable range in the degree of lateralization across the connectome. Some pathway-feature combinations showed a near-even split in directional preference across the population (i.e., median LI near 0 in **Figure 4** and % right-lateralized near 50% in **Figure 5**). Others exhibited strong and consistent lateralization, with 80-90% or more of individuals showing asymmetry in the same direction (e.g., AF and Striato-fronto-orbital [ST_FO] volume). Importantly, many of these distinct patterns were already clearly established in early childhood (3 years old).

Examining trends by feature type revealed broad patterns. For microstructure, FA was typically left-lateralized (negative LIs) across the population for most association tracts, with the main

exception being second branch of the fronto-parietal superior longitudinal fasciculus (SLF II), which tended to be right-dominant. In contrast, FA in projection tracts was more often right-lateralized in ~60-80% of the population. Other diffusivity measures (MD and AD) showed a modest but consistent leftward asymmetry across many pathways. For macrostructure, tract volume asymmetries were highly heterogeneous. Strong leftward lateralization (negative LIs) was evident for the AF (~75% of population) middle longitudinal fasiculus (MLF; ~95%), ST_FO (>95%), optic radiation (OR, ~85%), and the cingulum bundle (CG; ~80%). Strong rightward asymmetry (positive LIs) was observed for all branches (I, II, and III) of the fronto-parietal superior longitudinal fasciculus (SLF_I, 76-83%%; SLF_II, 89-91%; and SLF_III, 73-79%), and the uncinate fasciculus (UF, ~90%). Length also varied considerably; for instance, the length of AF was right-lateralized, whereas length of CG was left lateralized. Visual inspection of the heatmaps suggests these patterns are further modulated by age, a dynamic further explored in the final section.

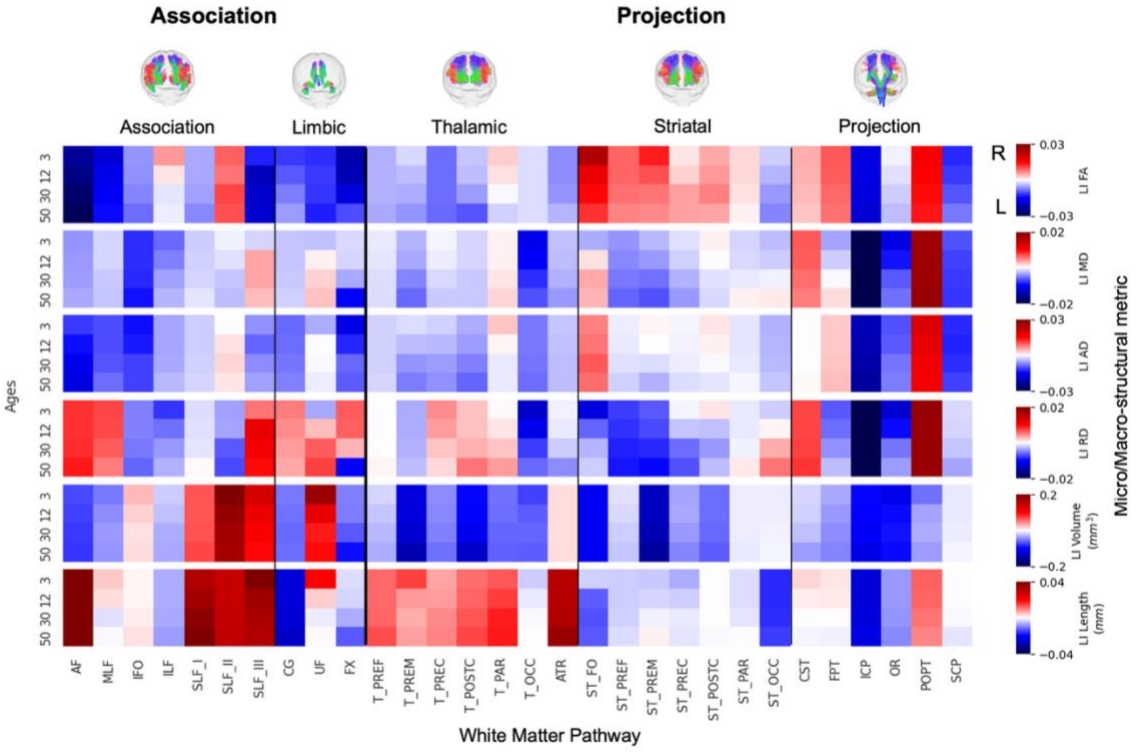

Figure 4. Population-level asymmetry at key lifespan milestones is highly specific to anatomical pathway and structural feature. Heatmaps depict the population-median Lateralization Index (LI) for six key features at four discrete age points (3, 12, 30, and 50 years) across 30 major white matter tracts. The color scale reflects the direction and magnitude of the median asymmetry (red: rightward; blue: leftward), highlighting that distinct patterns of lateralization are already established in early life and continue to evolve across the lifespan.

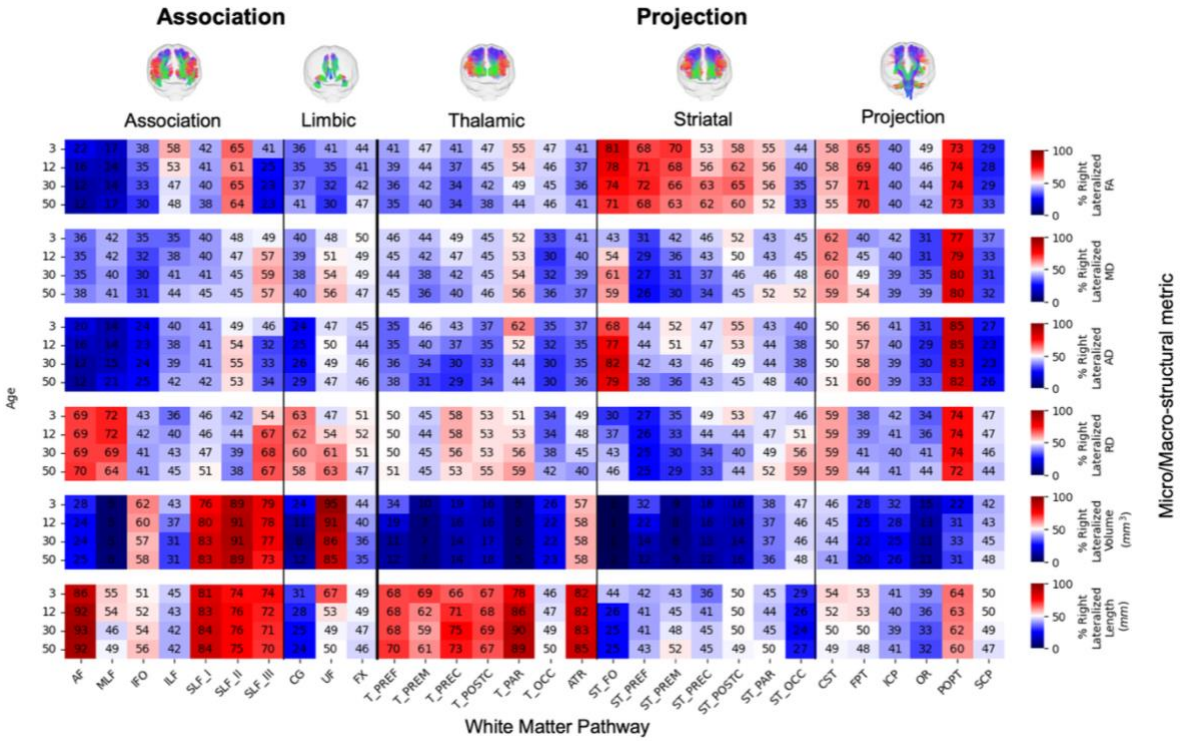

Figure 5. Population prevalence of rightward asymmetry across individuals. This figure complements **Figure 4** by showing the percentage of the population that is right-lateralized for the same features, tracts, and age points. Numerical values and the color scale indicate this prevalence (red: >50% right-lateralized; blue: <50% right-lateralized, i.e., majority left-lateralized). This visualization reveals the consistency of asymmetry across the population, demonstrating that even for tracts with a small median LI, a strong majority of individuals may share the same direction of lateralization.

Do asymmetries reverse direction across the lifespan?

Our analysis of the population median LI trajectories identified instances of "lateralization reversal," where the typical direction of (population-level) asymmetry shifts from one hemisphere to another across the lifespan (**Figure 6**). This indicates that hemispheric lateralization is not a fixed characteristic but can dynamically evolve with age. As shown in the figure, reversals in the median LI, though relatively sparse, are evident across all major tract groups. There are few patterns that generalize across all pathways or all features, although we note FA tends to reverse from right-to-left (if this occurs), whereas diffusivity measures generally show the opposite left-to-right trend. The timing of these population-level transitions varies considerably across the connectome. For instance, some median LIs reversed direction early in development, while others did so much later in life. This heterogeneity suggests complex and varying degrees of hemispheric plasticity over the lifespan, likely reflecting distinct underlying neurodevelopmental and neurodegenerative processes.

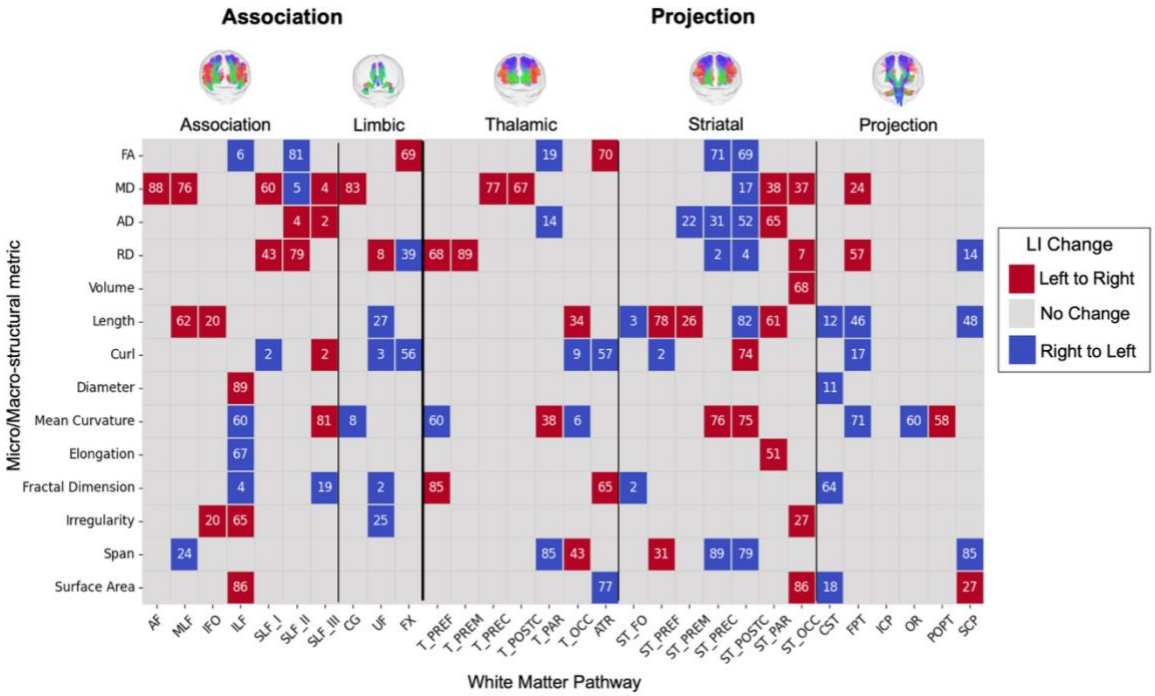

Figure 6. Lifespan trajectories reveal dynamic reversals in the direction of hemispheric asymmetry. Each cell indicates a "lateralization reversal," where the population-median LI for a given tract-feature combination crosses the zero line. Red cells indicate a transition from leftward to rightward asymmetry (negative to positive LI), while blue cells indicate a transition from rightward to leftward (positive to negative LI). The overlaid numbers represent the age (in years) at which this reversal occurs. The results demonstrate that while reversals are sparse, they occur across all major pathway types and at various life stages.

How does the magnitude of asymmetry evolve during different life stages?

Finally, we quantified how the magnitude of asymmetry evolves by calculating its rate of change (the slope of the absolute value of the median LI) within four distinct life stages: early/late childhood (2–12 years), adolescence (12–20 years), young adulthood (20–40 years), and middle/late adulthood (40–100 years). **Figure 7** shows these results, where an increasing asymmetry (greater |LI|, meaning *more* leftward or *more* rightward asymmetry) is indicated in red, and decreasing asymmetry (convergence towards symmetry, i.e., *less* leftward or *less* rightward) is shown in blue.

Childhood shows the most heterogenous patterns. Within the same feature class, some pathways show increasing symmetry while other show decreasing. For volume, increasing asymmetry is observed in AF, inferior longitudinal fasciculus (ILF), and several frontal/prefrontal connections (e.g., thalamo-prefrontal [T_PREF], ATR, FPT), whereas SLF-II, SLF-III, UF, and OR tend to decrease. For FA, increases appear in AF, SLF_III, and thalamo-premotor (T_PREM), while ST_FO, MLF, and ILF decrease. This mixture suggests active, pathway-specific refinement in childhood.

Adolescence largely continues the childhood directions but with smaller slopes (i.e., changes persist but are less pronounced), consistent with a tapering of developmental remodeling. Young

adulthood shows mostly modest shifts, with residual increases in selected macrostructural measures (volume and surface area standing out) and relatively small changes in diffusion metrics.

In middle/late adulthood, a trend emerges where the magnitude of asymmetry generally increases across a wide range of tracts and features. This effect was particularly strong for macrostructural measures like volume and surface area, which had generally been tending towards symmetry in earlier stages of development. For example, the MLF, UF, and nearly all projection pathways showed a strengthening of asymmetry in later life. In contrast, decreases in asymmetry (i.e., tracts becoming more symmetric) were less frequent, though notable exceptions were observed (including the volume of the SLF_II and SLF_III).

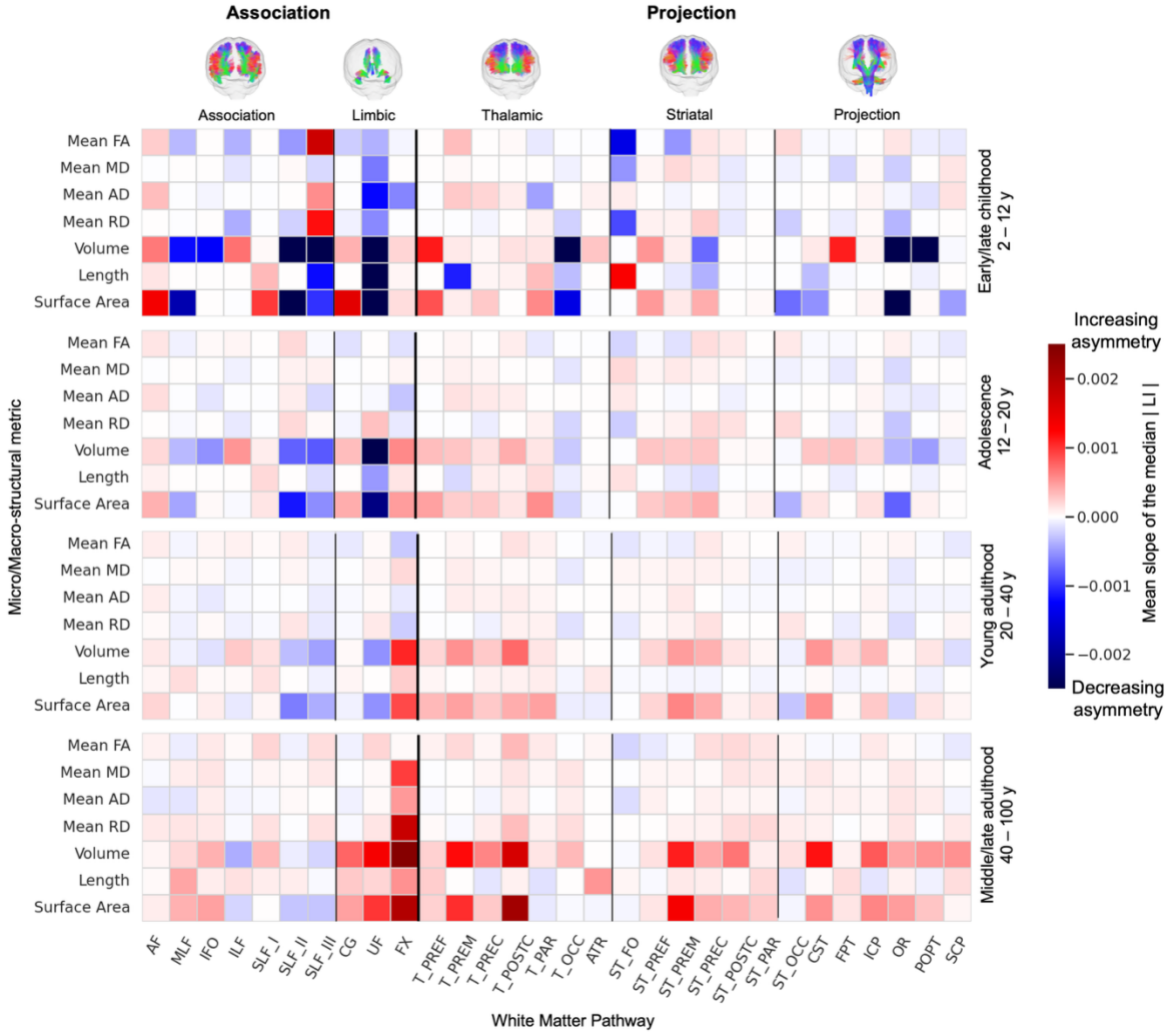

Figure 7. The evolution of asymmetry is a dynamic and age-specific process. This figure shows the mean rate of change (slope) of the population-median absolute lateralization index (|LI|) within four distinct life stages (rows). Each cell represents the slope for a given feature and white matter tract. Warmer colors (red) indicate an increase in the magnitude of asymmetry (strengthening of lateralization), while cooler colors (blue) denote a decrease in the magnitude of asymmetry (attenuation of lateralization). Childhood shows heterogeneous increases and decreases across pathways, adolescence largely continues these trends with smaller slopes, young adulthood is comparatively muted, and later adulthood shows a predominant increase—most marked for macrostructural measures (volume, surface area).

Discussion

This study represents the most comprehensive investigation of white matter asymmetry across the human lifespan. By leveraging a large-scale dataset of over 26,000 individuals from 42 neuroimaging cohorts, we generated normative lifespan trajectories for 14 distinct microstructural and macrostructural features across 30 lateralized long-range white matter pathways. Our principal findings reveal a complex and dynamic brain asymmetry across pathways, features, and the lifespan. First, we demonstrate that white matter asymmetries are widespread, affecting nearly all studied pathways, though the magnitude and lateralization vary considerably. Second, our results show that these asymmetries are feature-dependent, with different or even diverging patterns observed between measures of tissue microstructure and those reflecting pathway macrostructure. Third, we highlight that asymmetry profiles are pathway specific, likely reflecting the unique functional roles and developmental timelines of different neural pathways. Finally, we show that these asymmetries are not static but are highly dynamic, characterized by rapid, heterogeneous changes during childhood and a general trend of becoming more pronounced during the aging process. Together, these lifespan charts quantify the magnitude, direction, and age-specific variability of white-matter asymmetry, providing a reference to interpret individual differences and to study deviations in development, aging, and disease.

Widespread White Matter Asymmetry and Comparison with Prior Literature

Our study confirms and substantially extends the view of hemispheric asymmetry as a fundamental organizing principle of the brain's white matter connectome. By charting 30 pathways across the lifespan, we establish that asymmetries are common, yet heterogenous. A key insight from our normative modeling approach is the distinction between the *magnitude* of an asymmetry and its *consistency* across the population. While microstructural asymmetries often had modest population-median LIs, our centile charts reveal that even a small median effect can reflect a strong population consensus, with 70-90% of individuals showing the same directional asymmetry (**Figure 3**). Conversely, a larger median LI did not always guarantee unanimity. This highlights a critical limitation of relying on mean-based analyses alone and underscores the power of a distributional perspective for understanding brain lateralization.

These analyses also highlight that the nature and degree of asymmetry differ across both structural features and anatomical pathways, with many of these distinct lateralization patterns already evident in early infancy. Our lifespan perspective also revealed that inter-individual variability in asymmetry is not uniform (**Figure 3**, centile bands), with the widest centile bands observed in early childhood and in older age. This pattern likely reflects heterogeneous maturational rates and synaptic pruning during development,[41,42] and the cumulative impact of diverse genetic, environmental, and health-related factors during aging.[43]

Compared with prior reports studying asymmetry - typically smaller, age-restricted, and focused on a few tracts or metrics (**Table 2**, for a review of sample size and age range see **Supplementary Table 2**) - our lifespan curves generally corroborate well-established findings, such as the leftward FA and volumetric asymmetry of the arcuate fasciculus in adulthood, validating our large-scale harmonization. However, our data also help clarify previously conflicting reports in the literature[44], particularly for association pathways like the SLF, inferior fronto-occipital fasciculus (IFO), and UF. For the CST, some studies report left-lateralized microstructure,[22,45,46] whereas others (and

our results) indicate right-lateralized microstructure with left-lateralized macrostructure[45,47] - differences that likely reflect metric choice and age window.

Several factors explain discrepancies and the additional patterns detected here. First is scale: with N = 26,199, our centile modelling estimates population trajectories rather than relying on small-sample inference. Second, continuous age modelling (rather than single time points or assumption of homogeneity across age) exposes direction changes and non-linear trends that limited-age designs miss. Third, tract definition may vary across studies.[48] Automated, standardized segmentation (e.g., TractSeg)[31] reduces protocol variance but will not replicate every manual or atlas-based definition used previously. Finally, is the choice of features, as micro- and macrostructural features measure different aspects of pathway biology and can often diverge. By providing comprehensive, openly available lifespan asymmetry charts, our work offers a stable reference point to help reconcile these inconsistencies and guide future research.

Table 2. Comparison of our findings and those previously demonstrated in the literature. ✓ = agreement between our findings and those presented in the literature. X = disagreement between our findings and those presented in the literature. * (in "Findings") = tract or measure not measured in our work. * (in "Findings") + ✓/X = tract represented in our data as conglomerate or as multiple tracts, though still allowing for gross comparison. In cases where tract abbreviations presented in the literature differed from those of our tracts, we presented the tract name using our abbreviations.

Study	Age Range	Findings	Our Findings
Amemiya et al. (2021)	6–81 years	SLF III - FA - R	X
		SLF II - FA - R	✓
		SLF I - qR1 - L*	
Budisavljević et al. (2021)	18-29 years	SLF-degree-left (right-handers)*	
		SLF-degree-more symmetric (left-handers)*	
Gong et al. (2005)	20–40 years	CG - FA - L	✓
Schmithorst et al. (2008)	5–18 years	Splenium – FA – L (girls)*	
		AF – FA – R (boys)	X
		Frontal WM – FA – R (boys)*	
		Occipito-parietal WM – FA – R (boys)*	
		CST – MD – R (boys)	✓
		AF – MD – R (girls)	X
		Occipito-parietal WM – MD – R (girls)*	
Büchel et al. (2004)	21–43 years	AF–FA–L	✓
		CC–FA–R*	
		PreCG–FA–Contralateral to dominant hand	✓
Catani et al. (2007)	18–22 years	AF-FA-L	✓
Dayan et al. (2015)	5-18 years	OR-Volume-L	✓
		OR-RD-L	✓
		OR-MD-L	✓
		OR-AD-L	✓
		OR-FA-L (girls > boys)	✓
Demnitz et al. (2021)	62–70 years	CST-FA-L	X
		CST-MD-L	X
Honnedevasthana Arun et al. (2021)	22–35 years	SLF_I–FD–L*	
		SLF_II–FD–L*	
		SLF_IV–FD–R*	
		CG–FD–L*	
		IFOF–FD–R*	
		UF–FC–R*	
		ILF–FD–L*	
		OR–FD–L*	
		ICa–FD–R*	
		ICp–FD–L*	
		SFOF–FA–R*	
		ST–FA–R*	
		SCR–FA–L*	
Kumpulainen et al. (2023)	0–5 years	PTR-FA-L (infants)*	✓
		OR-FA-L (infants)	✓
		PCR-FA-L (infants)*	
		UNC-FA-R (infants)*	
		PLIC-FA-R (infants)*	
		ALIC-FA-R (infants)*	
		SCR-FA-R (infants)*	
		CG-FA-L (5 year-olds)	✓
		UF-FA-L (5 year-olds)	✓
		EC-FA-L (5 year-olds)*	
		SCR-FA-L (5 year-olds)*	
		ALIC-FA-R (5 year-olds)*	
		SFOF-FA-R (5 year-olds)*	
		ACR-FA-R (5 year-olds)*	
Glasser and Rilling (2008)	18–50 years	AF-FA-L	✓
Powell et al. (2006)	23-50 years	SLF-FA-L*	✓
		SLF-Volume-L*	X
		IFO-FA-L	✓
		IFO-Volume-L	X
		UF-FA-L	✓
		UF-Volume-L	X
Takao et al. (2011)	21-29 years	CC_anterior-FA-L*	
		CG-FA-L	✓
		OR-FA-L	✓
		SCP-FA-L	✓
		IC_anterior-FA-R*	
		UF-FA-R	X
		AF_superior-FA-R*	X
		AF_inferior-FA-R*	X
Thiebaut de Schotten et al. (2011)	Not noted	SLF_I-Volume-None	X
		SLF_II-Volume-R	✓
		SLF_III-Volume-R	✓
Hasan et al. (2009)	6 - 68 years	UF - FA - L	✓
		UF - AD - L	✓
Lebel and Beaulieu (2009)	5-30 years	AF - FA - L	✓
		AF - Streamlines - L*	
Dalamagkas et al. (2020)	22-35 years	CST – FA – no asymmetry	X
		HMFT – FA – R*	
Parekh et al. (2023)	8-12 years	ACR – AD - R*	
		AUC - FA - R*	
		AUC - AD - R*	
		AUC - MD - R*	
		CG - FA - L	✓
		CG - AD - L	✓
		CG - MD - R	X
		CG - RD – R	✓
		CP – FA- R*	
		CP – AD – R*	
		CP – MD – R*	
		CST – FA - L	X
		CST - MD - R	✓
		CST - RD - R	✓
		EC - FA - L*	
		EC - AD - R*	
		EC - MD - R*	
		EC - RD - R*	
		FX - AD - R	X
		FX - MD - R	X
		FX - RD - R	✓
		ICP - FA - R*	
		ICP - RD - L*	
		ML - FA - L*	
		ML - AD - R*	
		ML - MD - R*	
		ML - RD – R*	
		PCR – AD – R*	
		PCR – MD – R*	
		PCR – RD - R*	
		PLIC - FA - L*	
		PLIC - AD - R*	
		PLIC - MD - R*	
		PLIC - RD - R*	
		PTR – MD – R*	X
		PTR – RD - R*	✓
		RLIC - FA – L*	
		RLIC – AD - R*	
		RLIC - MD - R*	
		RLIC - RD - R*	
		SCP - FA - L	✓
		SCP - AD - R	X
		SCP - MD - R	X
		SCP - RD - R	X
		SCR - FA - L*	
		SCR - MD - R*	
		SCR - RD - R*	
		SFO – AD – R*	
		SFO – MD – R*	
		SLF - FA - L*	✓
		SLF - AD - R*	X
		SLF - MD - R*	X
		SLF - RD - R*	X
		SS - AD - R*	
		SS - MD - R*	
		SS - RD - R*	
		UF - FA - R	X
		UF - AD - R	X
		UF - RD - L	X
Putnam et al. (2010)	24-39 years	Splenium - FA - R*	
Sboto-Frankenstein et al. (2014)	19-30 years	FX - FA - L	✓
Shu et al. (2015)	23.4 ± 3.7 years 12 - 35 years (using 3 standard deviations)	AF – FA – L	✓
		ILF – FA – L	✓
		CB – FA – L*	
		IFO – FA – L	✓
		CB - Fiber Number - L*	
		OR - Fiber Number - R*	
		ILF - Fiber Number - L*	
		AF - Fiber Number - L*	
		UF - Fiber Number - R*	
Wu et al. (2016)	23-40 years	IFO - Volume - None	✓
Angstmann et al. (2016)	11-16 years	CST - FA - L	X
Barrick et al. (2007)	20-39 years	AF - FA - L	✓
Silk et al. (2016)	10-18 years	Caudate–VLPFC – volume – R*	
		Caudate–DLPFC – volume – R*	
Thiebaut de Schotten et al. (2011)	18-22 years	CST – volume – L	✓
		CST - streamlines - L*	
		OR – FA – R	X
		ILF–FA–L	✓
		IFOF–streamlines–R*	
		AF – volume – R	X
		AF_ant–volume–R*	
		AF_ant – streamlines – R*	
		AF_ant – FA - R*	
		AF_long–volume–L*	
		AF_long-streamlines-L*	
Vernooij et al. (2007)	25-54 years	AF-RFD-L*	
Wilde et al. (2009)	8-17 years	CG – FA – L	✓
		Post IC – FA – L*	
		Thalamus – FA – L*	
		Frontal WM – FA – L (males)*	
		Frontal WM - FA – R (females)*	
		Ant IC – FA – L (males)*	
		Ant IC - FA – *R (females)*	
Shu et al. (2021)	4-12 years	ATR - FA - R	X
		CST - FA - R	✓
		IFOF - FA - L	✓
		AF - FA - L	✓
Dubois et al. (2016)	6-22 weeks 21-27 years	AF - FA - L (infants)*	✓
		SLF - FA - L (infants)*	✓
		MLF - FA - L (infants)*	✓
		AF - AD - L (infants)*	✓
		SLF - AD - L (infants)*	X
		UF - AD - R (infants)*	X
		SLF - RD - R (infants)*	✓
		MLF - RD - R (infants)*	✓
		ILF - RD - L (infants)*	✓
		IFO - RD - L (infants)*	✓
Takao et al. (2013)	25 - 85 years	AF - Volume - L	✓
		CG - Volume - L	✓
		CC_genu - Volume - L*	
		IC - Volume - L*	
		SLF - Volume - L*	X
		EC - Volume - R*	
		AF - FA - L	✓
		CG_anterior - FA - L*	✓
		SLF - FA - L*	✓
Lebel et al. (2019)	4-33 years	AF-FA-L	✓
		IC-FA-L*	
		OR-FA-L	✓
		CG-FA-L	✓
		SLF-FA-L*	✓
		SCP-FA-L	✓
		UF-FA-L	✓
		Frontal-FA-R*	
		TR-FA-R*	
		Frontal-FA-L(child)-->R(adolescent)*	
Baudo et al. (2022)	20-40 years	AC_anterior – fiber projections – L*	
		AC_posterior – fiber projections – R*	
Briggs et al. (2020)	Not noted	FAT-volume-none*	
		IFO-volume-none	✓
		CG-volume-none	X
Ford et al. (2023)	0-1 years	AF – FA – L (1–3.5 mo)*	✓
		ATR – FA – R (3–6 mo)*	✓
		UF – FA – R (0–1.5 mo)*	X
		Fx – FA – L (5–6 mo)*	✓
		IFO – FA – L*	✓
		ILF – FA – R*	✓
		M1 – FA – L*	
		S1 – FA – R*	
		CG – FA – no asymmetry*	X
Hau et al. (2017)	22-34 years	UF_C1 – volume – L*	X
		UF_C3 – volume – R*	✓
		UF_C3 – streamline count – R*	
		UF_C5 – volume – R*	✓
Panesar et al. (2019)	23-35 years	vTPAT – connectivity – L*	
		dTPAT – connectivity – R*	
		AF – volume – L	✓
		SLF – volume – R	✓

Divergent Asymmetries of Microstructural and Macrostructural Features

Our findings demonstrate that white matter asymmetry is not "all encompassing" within a given pathway. Rather, it is highly feature dependent, meaning a tract broadly described as "left-lateralized" may not show leftward "dominance" for all its micro- and macrostructural characteristics. For instance, a pathway may exhibit leftward asymmetry for FA and other diffusivities (MD/AD) yet display rightward asymmetry for RD, as is seen in the arcuate fasciculus (AF) (**Figure 3**); or show leftward asymmetry in FA while its overall volume is greater in the right. These examples are widespread throughout our investigation (**Figures 4, 5**). This divergence highlights why simplistic labels such as "dominant" hemisphere for a tract or generalized statements about greater "white matter integrity" can be insufficient or even misleading without specifying which feature (reflecting distinct biological properties) is lateralized. Indeed, diffusion tensor metrics like FA and RD are sensitive to processes like myelination and axonal packing, AD to axonal structure and coherence, and MD to overall water diffusivity, each providing unique insights into pathways' structure[16]. The field must continue to investigate the biological and functional significance of these feature-specific asymmetries to better understand brain lateralization.

Pathway-Specific Patterns of White Matter Asymmetry

While previous work has generated such charts for grey matter[40] and white matter,[49] this is the first study to specifically chart asymmetry – creating population-level curves (describing the population-distribution) across age. From a basic neuroscience perspective, it provides insight into how neural circuits are lateralized in each hemisphere, lending evidence to the ongoing deduction of neuroanatomical structure-function relations.[10]

For example, established findings such as a denser, more coherent left AF (often reflected as greater FA) alongside a right-lateralized IFO volume have been interpreted as a structural basis for the left hemisphere's efficiencies in language processing versus the right's strengths in visuospatial integration.[50] Further illustrating these pathway-specific patterns, our data show that the SLF complex robustly demonstrated a strong rightward volume asymmetry, with typically 70-85% of the population exhibiting this pattern across the examined ages (**Figure 5**); this aligns with literature noting consistent rightward volume lateralization for segments like SLF_III, linked to right-hemisphere dominant visuospatial and attentional networks.[8,44] Moreover, such white matter asymmetries often parallel, and likely help to operationalize, established asymmetries in grey matter,[51-54] translating asymmetric cortical regions into functionally lateralized network dynamics. Our detailed findings on numerous pathways therefore lend further credence to the body of work exploring these critical structure-function relationships. This resource of asymmetrical reference distributions can guide future research aimed at more precisely linking specific structural asymmetries to individual differences in cognitive functions, behavioral traits, and susceptibility to or presentation of neurological or psychiatric disorders.

Dynamic Nature of Asymmetry Across the Lifespan

A central finding of this work is that white matter asymmetries are not static but follow dynamic trajectories across the lifespan (**Figure 3**). These dynamics are evident in both the population median LI trajectories and the corresponding population variability. While the typical magnitude of the median LI for many features, particularly microstructural ones, often remains within a

relatively constrained range (e.g., frequently staying below +/-0.1), especially during most of adult life, their specific values and trajectories show population-level changes over decades. This evolution varies considerably by pathway: some tracts exhibit clear shifts and modulations in their median asymmetry profiles across developmental and aging periods (e.g. which tracts), while others maintain a more consistent pattern of lateralization and population distribution throughout much of life (e.g. AF). The periods of most pronounced change in these asymmetry trajectories - reflecting significant neural reorganization generally occur during very early development and again in later life during healthy aging. It is important to highlight the cross-sectional nature of the current dataset; because of this, we cannot (or do not) follow individual "change" but rather cross-sectional median and ranges across the population.

We also demonstrate, for the first time to our knowledge, the presence of "lateralization reversal", where the typical direction of asymmetry for a given feature shifts across the lifespan. This phenomenon occurred in almost every tract we measured and for at least one, and often more, measures of connectivity (**Figure 6**), although the overall frequency was indeed sparse across pathways and features. While previous studies have demonstrated patterns of development of asymmetry over short age ranges,[55-57] identifying specific reversal points is possible by including data across the entire lifespan. The neurodevelopmental and clinical significance of this phenomenon is, to our knowledge, completely unexplored.

Finally, our analysis reveals another novel lifespan trend: the degree of white matter asymmetry shows a general tendency to increase from mid-life to old age (**Figure 7**). While asymmetry in infancy/development has been a focus of prior research,[58] its evolution during aging is less understood with limited prior investigations.[22] Our results demonstrate that several features (volume, diameter, elongation, irregularity, and surface area) become more asymmetric with age across most pathways, and many other features show similar trends. We hypothesize that these findings are reflective of natural age-related neurodegenerative processes – occurring in individuals over 50 years old – where one hemisphere's pathways (or specific aspects of their structure) are more vulnerable or decline at a faster rate than their contralateral counterpart, leading to the amplifying initial subtle asymmetries. Future studies are crucial to determine the neurocognitive and clinical impact, if any, of these age-related increases in white matter asymmetry.

Functional Implications and Clinical Relevance of White Matter Asymmetry

Our findings also carry potential clinical implications. As research accumulates, white matter asymmetry measures could serve as biomarkers for certain conditions such as schizophrenia[59] and Parkinson's disease[27] or as indices of typical vs. atypical brain development, such as in autism spectrum disorder.[60] Asymmetry is a particularly attractive biomarker since it is inherently normalized to the individual via its computation as ratios or differences within the same scan. In children with neurodevelopmental disorders, it has been demonstrated that lateralization indices of diffusion metrics might serve as clinically useful imaging biomarkers, helping to detect sensory processing dysfunction with less confounding variance than absolute measures.[45] In neurodegenerative diseases, asymmetry often manifests as an asymmetrical onset of pathology. Parkinson's disease typically begins with unilateral motor deficits (reflecting greater degeneration of one side's nigrostriatal pathway), and patients correspondingly show asymmetric cortical changes in several hemispheric regions[61]; a similar investigation into asymmetrical changes in

white matter structural connectivity has not yet been conducted. With continued development, detection of such asymmetry measures can complement other markers to improve early detection of atypical brain development or pathology.

The role of asymmetry across disease states has only begun to be characterized. When considering clinical populations, white matter asymmetry has been a topic of intense investigation. Research in autism, for example, has observed that typical lateralization patterns are often reduced or altered. Children with autism spectrum disorer have been shown to have significantly diminished asymmetry of white matter microstructure, with many of the normal left-right differences in FA, AD, and RD being smaller in magnitude in autism spectrum disorder, indicating a more symmetrical white matter organization.[19,24] Schizophrenia is another condition where white matter asymmetry is studied: some patients show a reduction or reversal of asymmetry in the AF and SLF, among others, with reduced asymmetry in the FA being seen in patients experiencing auditory hallucinations,[62] possibly underlying the disturbed lateralization of language processing in schizophrenia.[24] In such investigations of pathology-associated asymmetries, our work can serve as a cornerstone for future comparisons. By providing a multitude of tracts and measures modeled across the lifespan, our charts can reasonably be used as healthy controls in any study which seeks to investigate a particular tract, connectivity measure, and/or critical age range in an abnormal brain state. Our findings in healthy controls, therefore, potentially enables the discovery of different asymmetries that arise in pathological states, providing insight into the mechanism of a given disease.

Limitations

Our study had notable limitations. We note the results for the fornix (FX) should be interpreted with caution as they could be a result of technical tractography artifacts rather than a biological changes; while this is particularly true of FX, such considerations can be grossly applied to all tractography methods. Macrostructural features are susceptible to the methods used to grid data and so can vary between studies. Similarly, different protocols for delineation of pathways can lead to different regions being included or excluded from a given pathway, lending further complexity to the matter of comparing study results. Lastly, there is overlap in the regions which define given pathways, meaning that microstructural measures in those regions are not unique to the given pathway.

Conclusion

This study provides the most extensive characterization of white matter asymmetry across the human lifespan to date, generating comprehensive normative trajectories for 14 structural features across 30 distinct white matter pathways in over 26,000 healthy individuals from infancy to old age. Our key findings demonstrate that white matter asymmetries are widespread yet highly specific to pathways and structural features. Furthermore, these asymmetries are not static but exhibit dynamic changes throughout development and aging, including reversals in direction and a general trend of increasing asymmetry magnitude in later life. These lifespan charts of white matter asymmetry offer a resource for advancing our understanding of brain lateralization

principles, investigating inter-individual variability in brain structure, and providing a reference to assess deviations in neurodevelopmental, aging, and clinical populations.

Data Availability

Population curves for each pathway and each feature are in format npy and available on Zenodo *[XXXXXXXXXXX]*. Code for GAMLLS fitting is at https://github.com/MASILab/Asymmetry/blob/main/src/fit_model.py, code to generate figures is at https://github.com/MASILab/Asymmetry/blob/main/src/plot_fit.ipynb. Additionally, the GAMLLS models for each pathway and each feature are available on Zenodo upon publication.

Conflict of Interest

The authors declare that they have no conflict of interest.

Declaration of Generative AI and AI-assisted Technologies in the Writing Process

During the preparation of this work the authors used ChatGPT, an AI language model developed by OpenAI, and Gemini, an AI language model developed by Google, in order to assist in rephrasing the text in this paper for clarification. After using this tool, the authors reviewed and edited the content as needed and takes full responsibility for the content of the publication.

Acknowledgements and Funding

This work was supported in part by the National Institute of Health through NIH awards K01-EB032898 (Schilling) and K01-AG073584 (Archer), grant number 1R01EB017230-01A1 (Landman), K24-AG046373 (Jefferson), and ViSE/VICTR VR3029, UL1-TR000445, and UL1-TR002243. This work was supported by NIA grants R01-AG034962 (Jefferson), R01-AG056534 (Jefferson), R01-AG062826, and Alzheimer's Association IIRG-08-88733 (Jefferson) and the NICHD, R01-HD114489 (Vinci-Booher). This work was supported by the Alzheimer's Disease Sequencing Project Phenotype Harmonization Consortium (ADSP-PHC) that is funded by NIA (U24 AG074855, U01 AG068057 and R01 AG059716). This work was conducted in part using the resources of the Advanced Computing Center for Research and Education (ACCRE) at Vanderbilt University, Nashville, TN. We appreciate the National Institute of HealthS10 Shared Instrumentation grant 1S10OD020154-01, and grant 1S10OD023680-01 (Vanderbilt's High-Performance Computer Cluster for Biomedical Research). This work was also supported in part by Intramural Research Program of the National Institute on Aging, NIH.

Research reported in this publication was supported by NIGMS of the National Institutes of Health under award number T32GM007347 and T32GM152284.

This work was supported by the Donders Mohrmann Fellowship on 'Neurovariability' No. 2401515 (Stephanie J. Forkel) and the Dutch Research Council NWO Aspasia Grant 'Human individuality: phenotypes, cognition, and brain disorders' (Stephanie J. Forkel).

Data and/or research tools used in the preparation of this manuscript were obtained from the National Institute of Mental Health (NIMH) Data Archive (NDA). NDA is a collaborative informatics system created by the National Institutes of Health to provide a national resource to support and accelerate research in mental health. This manuscript reflects the views of the authors and may not reflect the opinions or views of the NIH or of the Submitters submitting original data to NDA.

This research was supported by the Intramural Research Program of the NIH, National Institute on Aging. The contributions of the NIH authors were made as part of their official duties as NIH federal employees, are in compliance with agency policy requirements, and are considered Works of the United States Government. However, the findings and conclusions presented in this paper are those of the authors and do not necessarily reflect the views of the NIH or the U.S. Department of Health and Human Services.

We acknowledge the data provided by several initiatives:

HABS-HD: Research reported on this publication was supported by the National Institute on Aging of the National Institutes of Health under Award Numbers R01AG054073, R01AG058533, R01AG070862, P41EB015922 and U19AG078109. The content is solely the responsibility of the authors and does not necessarily represent the official views of the National Institutes of Health.

PING: The Pediatric Imaging, Neurocognition, and Genetics (PING) dataset was collected and released openly to contribute to the assessment of typical brain development in a pediatric sample (RC2DA029475-01), (https://www.sciencedirect.com/science/article/pii/S1053811915003572).

HCP: The data used in this study come from the Human Connectome Project, which aims to map the structural connections and circuits of the brain and their relationships to behavior by acquiring high-quality magnetic resonance images. We used diffusion MRI data from the Baby Connectome Project (HCPBaby), the Human Connectome Project Development (HCPD) study, the Human Connectome Project Young Adult (HCP) study, and the Human Connectome Project Aging (HCPA) study.

Research data from the Infant Brain Imaging Study (IBIS) dataset come from the IBIS Autism project, a collaborative effort by investigators to conduct a longitudinal MRI/DTI and behavioral study of infants at high risk for autism (R01HD055741-01).

NKI-RS: The Enhanced NKI-RS is a large cross-sectional sample of brain development, maturation and aging, that is currently funded by the NIMH (BRAINS R01MH094639-01; PI Milham) and Child Mind Institute (PI Milham) to characterize 1000 community-ascertained participants using state-of-the-art multiplex imaging-based resting state fMRI (R-fMRI) and diffusion tensor imaging (DTI), genetics, and a broad neurobehavioral phenotypic characterization protocol. Data were acquired from the DSI studio website: (https://brain.labsolver.org/nki_rockland.html).

HBN: The Healthy Brain Network (HBN) is an ongoing initiative focused on building a biobank of data from 10,000 children and adolescents (ages 5-21) in the New York City area (https://www.nature.com/articles/sdata2017181). Data were acquired from the DSI studio website: (https://brain.labsolver.org/hbn.html).

Humphreys: This work was supported by the Jacobs Foundation Early Career Research Fellowship (2017-1261-05) (Humphreys); National Science Foundation CAREER Award (2042285) (Humphreys); Brain and Behavior Research Foundation John and Polly Sparks Foundation Investigator Award (29593) (Humphreys); Vanderbilt Institute for Clinical and Translational Research Grant (VR53419) (Humphreys); Vanderbilt Strong Grant; Vanderbilt Kennedy Center Grant (Humphreys); National Institute of Mental Health (R01MH129634) (Humphreys).

ADNI: Data used in the preparation of this article were obtained from the Alzheimer's Disease Neuroimaging Initiative (ADNI) database (adni.loni.usc.edu). The ADNI was launched in 2003 as a public-private partnership, led by Principal Investigator Michael W. Weiner, MD. The primary goal of ADNI has been to test whether serial magnetic resonance imaging (MRI), positron emission tomography (PET), other biological markers, and clinical and neuropsychological assessment can be combined to measure the progression of mild cognitive impairment (MCI) and early Alzheimer's disease (AD).

Data collection and sharing for ADNI were supported by National Institutes of Health Grant U01-AG024904 and Department of Defense (award number W81XWH-12-2-0012). ADNI is also funded by the National Institute on Aging, the National Institute of Biomedical Imaging and Bioengineering, and through generous contributions from the following: AbbVie, Alzheimer's Association; Alzheimer's Drug Discovery Foundation; Araclon Biotech; BioClinica, Inc.; Biogen; Bristol-Myers Squibb Company; CereSpir, Inc.; Cogstate; Eisai Inc.; Elan Pharmaceuticals, Inc.; Eli Lilly and Company; EuroImmun; F. Hoffmann-La Roche Ltd and its affiliated company Genentech, Inc.; Fujirebio; GE Healthcare; IXICO Ltd.; Janssen Alzheimer Immunotherapy Research & Development, LLC.; Johnson & Johnson Pharmaceutical Research & Development LLC.; Lumosity; Lundbeck; Merck & Co., Inc.; Meso Scale Diagnostics, LLC.; NeuroRx Research; Neurotrack Technologies; Novartis Pharmaceuticals Corporation; Pfizer Inc.; Piramal

Imaging; Servier; Takeda Pharmaceutical Company; and Transition Therapeutics. The Canadian Institutes of Health Research is providing funds to support ADNI clinical sites in Canada. Private sector contributions are facilitated by the Foundation for the National Institutes of Health (www.fnih.org). The grantee organization is the Northern California Institute for Research and Education, and the study is coordinated by the Alzheimer's Therapeutic Research Institute at the University of Southern California. ADNI data are disseminated by the Laboratory for Neuro Imaging at the University of Southern California.

VMAP: Study data were obtained from the Vanderbilt Memory and Aging Project (VMAP). VMAP data were collected by Vanderbilt Memory and Alzheimer's Center Investigators at Vanderbilt University Medical Center. This work was supported by NIA grants R01-AG034962 (PI: Jefferson), R01-AG056534 (PI: Jefferson), R01-AG062826 (PI: Gifford), and Alzheimer's Association IIRG-08-88733 (PI: Jefferson).

BLSA: The BLSA is supported by the Intramural Research Program, National Institute on Aging, NIH. BLSA is a prospective cohort study with continuous enrollment that began in 1958. Comprehensive data from BLSA are available upon request by a proposal submission through the cohort website (www.blsa.nih.gov).

BIOCARD: The BIOCARD study is designed to identify biomarkers associated with progression from normal cognitive status to cognitive impairment or dementia, with a particular focus on Alzheimer's Disease. The BIOCARD study is supported by a grant from the National Institute on Aging (NIA): U19-AG03365. The BIOCARD Study consists of 7 Cores and 2 projects with the following members: (1) The Administrative Core (Marilyn Albert, Corinne Pettigrew, Barbara Rodzon); (2) the Clinical Core (Marilyn Albert, Anja Soldan, Rebecca Gottesman, Corinne Pettigrew, Leonie Farrington, Maura Grega, Gay Rudow, Rostislav Brichko, Scott Rudow, Jules Giles, Ned Sacktor); (3) the Imaging Core (Michael Miller, Susumu Mori, Anthony Kolasny, Hanzhang Lu, Kenichi Oishi, Tilak Ratnanather, Peter vanZijl, Laurent Younes); (4) the Biospecimen Core (Abhay Moghekar, Jacqueline Darrow, Alexandria Lewis, Richard O'Brien); (5) the Informatics Core (Roberta Scherer, Ann Ervin, David Shade, Jennifer Jones, Hamadou Coulibaly, Kathy Moser, Courtney Potter); the (6) Biostatistics Core (Mei-Cheng Wang, Yuxin Zhu, Jiangxia Wang); (7) the Neuropathology Core (Juan Troncoso, David Nauen, Olga Pletnikova, Karen Fisher); (8) Project 1 (Paul Worley, Jeremy Walston, Mei-Fang Xiao), and (9) Project 2 (Mei-Cheng Wang, Yifei Sun, Yanxun Xu.

UK Biobank: This research has been conducted using the UK Biobank resource, application 16315.

CamCAN: Data collection and sharing for this project was provided by the Cambridge Centre for Ageing and Neuroscience (CamCAN). CamCAN funding was provided by the UK Biotechnology and Biological Sciences Research Council (grant number BB/H008217/1), together with support from the UK Medical Research Council and University of Cambridge, UK. Data used in the preparation of this work were obtained from the CamCAN repository (available at http://www.mrc-cbu.cam.ac.uk/datasets/camcan/). The Cambridge Centre for Ageing and Neuroscience (Cam-CAN) is a large-scale collaborative research project at the University of Cambridge.

HBN: The Healthy Brain Network (HBN) is an ongoing initiative focused on building a biobank of data from 10,000 children and adolescents (ages 5-21) in the New York City area

(https://www.nature.com/articles/sdata2017181). Data were acquired from the DSI studio website: (https://brain.labsolver.org/hbn.html).

MAP/ROS/MARS: Data contributed from MAP/ROS/MARS was supported by NIA R01AG017917, P30AG10161, P30AG072975, R01AG022018, R01AG056405, UH2NS100599, UH3NS100599, R01AG064233, R01AG15819 and R01AG067482, and the Illinois Department of Public Health (Alzheimer's Disease Research Fund). Data can be accessed at

www.radc.rush.edu. More information about participant demographics and study information can be found here: https://www.rushu.rush.edu/research-rush-university/departmental-research/rush-alzheimers-disease-center/rush-alzheimers-disease-center-research/epidemiologic-research.

The data contributed from the Wisconsin Registry for Alzheimer's Prevention was supported by NIA AG021155, AG0271761, AG037639, and AG054047.

MORGAN: Data collected from the MORGAN dataset were acquired at Vanderbilt University, with the aim of studying cognitive patterns in epileptic patients both before and after clinical treatment for epilepsy.

CALM: Data collection and sharing for this project was provided by the Centre for Attention, Learning and Memory (CALM). CALM funding was provided by the UK Medical Research Council and University of Cambridge, UK. Data used in the preparation of this work were obtained from CALM resource – https://calm.mrc-cbu.cam.ac.uk/. The study protocol is reported in Holmes et al. (2019).

UTAustin: The dataset that we refer to as UTAustin in this manuscript is a longitudinal neuroimaging dataset on language processing in children ages 5, 7, and 9 years old collected at The University of Texas at Austin. The dataset is openly available from Openneuro here: https://openneuro.org/datasets/ds003604/versions/1.0.7. We use version 1.0.7.

QTAB: The Queensland Twin Adolescent Brain (QTAB) Project was established with the purpose of promoting the conduct of health-related research in adolescence. The QTAB dataset comprises multimodal neuroimaging, as well as cognitive and mental health data collected in adolescent twins over two sessions. The MRI protocol consisted of T1-weighted (MP2RAGE), T2-weighted, FLAIR, high-resolution TSE, SWI, resting-state fMRI, DWI, and ASL scans. The QTAB project resource was produced as a result of i) the goodwill and contribution of 422 twin/triplet participants and their parents, ii) funding from the National Health and Medical Research Council, Australia (APP1078756) and the Queensland Brain Institute, University of Queensland, iii) access to several key resources, including the Centre for Advanced Imaging, the Human Studies Unit, Institute of Molecular Bioscience, and the Queensland Cyber Infrastructure Foundation, at the University of Queensland, local and national twin registries at the QIMR Berghofer Medical Research Institute and Twin Research Australia, as well as the many assessments made available by researchers worldwide, and iv) was established with the purpose of promoting the conduct of health-related research in adolescence. The imaging data and basic demographics are openly accessibly on Openneuro here: https://openneuro.org/datasets/ds004146/versions/1.0.4. We use version 1.0.4.

TempleSocial: The Social Reward and Nonsocial Reward Processing Across the Adult Lifespan: An Interim Multi-echo fMRI and Diffusion Dataset (referred to as TempleSocial in this manuscript) comes from a study that aims to investigate whether older adults have a blunted response to some features of social reward. The dataset is openly accessibly on Openneuro here: https://openneuro.org/datasets/ds005123/versions/1.1.3. In particular, we use version 1.1.3.

Lexical: The Longitudinal Brain Correlates of Multisensory Lexical Processing in Children study (shortened to Lexical in this manuscript) aims to explore developmentally dependent changes in lexical processing for adolescents. The dataset is openly accessibly on Openneuro here: https://openneuro.org/datasets/ds001894/versions/1.4.2. We use version 1.4.2.

Lac5: The UCLA Consortium for Neuropsychiatric Phenomics LA5c Study (UCLA Lac5) is focused on understanding the dimensional structure of memory and cognitive control (response inhibition) functions in both healthy individuals and individuals with neuropsychiatric disorders including schizophrenia, bipolar disorder, and attention deficit/hyperactivity disorder. Neuroimaging data were downloaded from Openneuro here: https://openneuro.org/datasets/ds000030/versions/1.0.0. We use version 1.0.0.

UpennRisk: The dataset we refer to as UPennRisk comes from a study at University of Pennsylvania that investigated whether training executive cognitive function could influence choice behavior and brain responses. Neuroimaging data were downloaded from Openneuro here: https://openneuro.org/datasets/ds002843/versions/1.0.1. We use version 1.0.1.

DLBS: The Dallas Lifespan Brain Study (DLBS) is a longitudinal multi-modal neuroimaging study of the aging mind, which was initiated in 2008 (referred to as Wave 1). Participants returned for two additional waves of data collection with an approximate interval of 4-5 years between waves. The DLBS protocol encompasses various imaging modalities, including structural MRI, diffusion MRI, and functional MRI, as well as comprehensive cognitive and psychosocial assessments. DLBS data can be downloaded from Openneuro here: https://openneuro.org/datasets/ds004856. Specifically, we use version 1.2.0.

MASiVar: The Multisite, Multiscanner, and Multisubject Acquisitions for Studying Variability in Diffusion Weighted Magnetic Resonance Imaging (MASiVar) dataset consists of 319 diffusion scans acquired at 3T from b = 1000 to 3000 s/mm2 across 14 healthy adults, 83 healthy children (5 to 8 years), three sites, and four scanners curated to promote investigation of diffusion MRI variability. In particular, we used only the data coming from healthy children (Cohort IV) for version 2.0.2 of the dataset. Data are available to download from Openneuro here: https://openneuro.org/datasets/ds003416/versions/2.0.2.

SWU: Data coming from the Southwestern University (SWU) dataset, part of the Consortium for Reliability and Reproducibility (CoRR), were downloaded via NITRC-IR from the 1000 Functional Connectomes Project. Specifically, the data come from the Emotion and Creativity One Year Retest Dataset subset, comprised of 235 subjects, all of whom were college students. Each subject underwent two sessions of anatomical, resting state fMRI, and DTI scans, spaced one year apart. In order to access the CoRR datasets through NITRC, users must be logged into NITRC at the time of download and registered with the 1000 Functional Connectomes Project / INDI website. More information about this subset can be found here: https://fcon_1000.projects.nitrc.org/indi/CoRR/html/swu_4.html.

Calgary: The Preschool MRI study in The Developmental Neuroimaging Lab at the University of Calgary (https://www.developmentalneuroimaginglab.ca) uses different magnetic resonance imaging (MRI) techniques to study brain structure and function in early childhood. The study aims to characterize brain development in early childhood, and to offer baseline data that can be used to understand cognitive and behavioural development, as well as to identify deviations from normal development in children with various diseases, disorders, or brain injuries. The MRI techniques used include diffusion tensor imaging (DTI), anatomical imaging, arterial spin labeling

(ASL), and resting state functional MRI (rsfMRI). Data can be downloaded from here: https://osf.io/axz5r/.

CUTTING: This work was supported by the National Institute of Child Health and Human Development (NICHD) through awards R01 HD089474 (Cutting), R37 HD095519 (Cutting), R01 HD044073 (Cutting), and R01 HD067254 (Cutting). This work was supported by the Vanderbilt Kennedy Center funded by NICHD through award P50 HD103537. This work utilized REDCap supported by the National Center for Advancing Translational Sciences (NCATS) through award UL1 TR000445 to the Vanderbilt Institute for Clinical and Translational Research. This work was supported by the National Institute of Health's Office of the Director (1S10 OD021771-01) to the Vanderbilt University Institute of Imaging Science.

AOMIC: The Amsterdam Open MRI Collection (AOMIC) is a collection of three datasets with multimodal (3T) MRI data including structural (T1-weighted), diffusion-weighted, and (resting-state and task-based) functional BOLD MRI data, as well as detailed demographics and psychometric variables from a large set of healthy participants. All raw data is publicly available from the Openneuro data sharing platform: ID1000: https://openneuro.org/datasets/ds003097, PIOP1: https://openneuro.org/datasets/ds002785, PIOP2: https://openneuro.org/datasets/ds002790. We use version 1.2.1 for ID1000 and 2.0.0 for PIOP1 and PIOP2.

BANDA: The Boston Adolescent Neuroimaging of Depression and Anxiety (BANDA) is a study of 215 adolescents ages 14-17, 152 of whom had a current diagnosis of a DSM-5 (APA, 2013) anxious and/or depressive disorder. The BANDA study collected a rich dataset of brain, clinical, and cognitive/neuropsychological measures from these adolescent subjects. The dataset is available to download upon request on the NDA.

ADRC: We thank Knight ADRC for providing neuroimaging data to us. The data contributed through WASHU (Knight ADRC) was supported by grant numbers P30 AG066444, P01 AG03991, and P01 AG026276. For WASHU, Clinical Dementia Ratings (CDRs) are obtained from assessments by experienced clinicians trained in the use of the CDR.

NACC: The NACC database is funded by NIA/NIH Grant U24 AG072122. NACC data are contributed by the NIA-funded ADRCs: P30 AG062429 (PI James Brewer, MD, PhD), P30 AG066468 (PI Oscar Lopez, MD), P30 AG062421 (PI Bradley Hyman, MD, PhD), P30 AG066509 (PI Thomas Grabowski, MD), P30 AG066514 (PI Mary Sano, PhD), P30 AG066530 (PI Helena Chui, MD), P30 AG066507 (PI Marilyn Albert, PhD), P30 AG066444 (PI John Morris, MD), P30 AG066518 (PI Jeffrey Kaye, MD), P30 AG066512 (PI Thomas Wisniewski, MD), P30 AG066462 (PI Scott Small, MD), P30 AG072979 (PI David Wolk, MD), P30 AG072972 (PI Charles DeCarli, MD), P30 AG072976 (PI Andrew Saykin, PsyD), P30 AG072975 (PI David Bennett, MD), P30 AG072978 (PI Ann McKee, MD), P30 AG072977 (PI Robert Vassar, PhD), P30 AG066519 (PI Frank LaFerla, PhD), P30 AG062677 (PI Ronald Petersen, MD, PhD), P30 AG079280 (PI Eric Reiman, MD), P30 AG062422 (PI Gil Rabinovici, MD), P30 AG066511 (PI Allan Levey, MD, PhD), P30 AG072946 (PI Linda Van Eldik, PhD), P30 AG062715 (PI Sanjay Asthana, MD, FRCP), P30 AG072973 (PI Russell Swerdlow, MD), P30 AG066506 (PI Todd Golde, MD, PhD), P30 AG066508 (PI Stephen Strittmatter, MD, PhD), P30 AG066515 (PI Victor Henderson, MD, MS), P30 AG072947 (PI Suzanne Craft, PhD), P30 AG072931 (PI Henry Paulson, MD, PhD), P30 AG066546 (PI Sudha Seshadri, MD), P20 AG068024 (PI Erik Roberson,

MD, PhD), P20 AG068053 (PI Justin Miller, PhD), P20 AG068077 (PI Gary Rosenberg, MD), P20 AG068082 (PI Angela Jefferson, PhD), P30 AG072958 (PI Heather Whitson, MD), P30 AG072959 (PI James Leverenz, MD).

SCAN is a multi-institutional project that was funded as a U24 grant (AG067418) by the National Institute on Aging in May 2020. Data collected by SCAN and shared by NACC are contributed by the NIA-funded ADRCs as follows: Arizona Alzheimer's Center - P30 AG072980 (PI: Eric Reiman, MD); R01 AG069453 (PI: Eric Reiman (contact), MD); P30 AG019610 (PI: Eric Reiman, MD); and the State of Arizona which provided additional funding supporting our center; Boston University - P30 AG013846 (PI Neil Kowall MD); Cleveland ADRC - P30 AG062428 (James Leverenz, MD); Cleveland Clinic, Las Vegas – P20AG068053; Columbia - P50 AG008702 (PI Scott Small MD); Duke/UNC ADRC – P30 AG072958; Emory University - P30AG066511 (PI Levey Allan, MD, PhD); Indiana University - R01 AG19771 (PI Andrew Saykin, PsyD); P30 AG10133 (PI Andrew Saykin, PsyD); P30 AG072976 (PI Andrew Saykin, PsyD); R01 AG061788 (PI Shannon Risacher, PhD); R01 AG053993 (PI Yu-Chien Wu, MD, PhD); U01 AG057195 (PI Liana Apostolova, MD); U19 AG063911 (PI Bradley Boeve, MD); and the Indiana University Department of Radiology and Imaging Sciences; Johns Hopkins - P30 AG066507 (PI Marilyn Albert, Phd.); Mayo Clinic - P50 AG016574 (PI Ronald Petersen MD PhD); Mount Sinai - P30 AG066514 (PI Mary Sano, PhD); R01 AG054110 (PI Trey Hedden, PhD); R01 AG053509 (PI Trey Hedden, PhD); New York University - P30AG066512-01S2 (PI Thomas Wisniewski, MD); R01AG056031 (PI Ricardo Osorio, MD); R01AG056531 (PIs Ricardo Osorio, MD; Girardin Jean-Louis, PhD); Northwestern University - P30 AG013854 (PI Robert Vassar PhD); R01 AG045571 (PI Emily Rogalski, PhD); R56 AG045571, (PI Emily Rogalski, PhD); R01 AG067781, (PI Emily Rogalski, PhD); U19 AG073153, (PI Emily Rogalski, PhD); R01 DC008552, (M.-Marsel Mesulam, MD); R01 AG077444, (PIs M.-Marsel Mesulam, MD, Emily Rogalski, PhD); R01 NS075075 (PI Emily Rogalski, PhD); R01 AG056258 (PI Emily Rogalski, PhD); Oregon Health and Science University - P30 AG008017 (PI Jeffrey Kaye MD); R56 AG074321 (PI Jeffrey Kaye, MD); Rush University - P30 AG010161 (PI David Bennett MD); Stanford – P30AG066515; P50 AG047366 (PI Victor Henderson MD MS); University of Alabama, Birmingham – P20; University of California, Davis - P30 AG10129 (PI Charles DeCarli, MD); P30 AG072972 (PI Charles DeCarli, MD); University of California, Irvine - P50 AG016573 (PI Frank LaFerla PhD); University of California, San Diego - P30AG062429 (PI James Brewer, MD, PhD); University of California, San Francisco - P30 AG062422 (Rabinovici, Gil D., MD); University of Kansas - P30 AG035982 (Russell Swerdlow, MD); University of Kentucky - P30 AG028283-15S1 (PIs Linda Van Eldik, PhD and Brian Gold, PhD); University of Michigan ADRC - P30AG053760 (PI Henry Paulson, MD, PhD) P30AG072931 (PI Henry Paulson, MD, PhD) Cure Alzheimer's Fund 200775 - (PI Henry Paulson, MD, PhD) U19 NS120384 (PI Charles DeCarli, MD, University of Michigan Site PI Henry Paulson, MD, PhD) R01 AG068338 (MPI Bruno Giordani, PhD, Carol Persad, PhD, Yi Murphey, PhD) S10OD026738-01 (PI Douglas Noll, PhD) R01 AG058724 (PI Benjamin Hampstead, PhD) R35 AG072262 (PI Benjamin Hampstead, PhD) W81XWH2110743 (PI Benjamin Hampstead, PhD) R01 AG073235 (PI Nancy Chiaravalloti, University of Michigan Site PI Benjamin Hampstead, PhD) 1I01RX001534 (PI Benjamin Hampstead, PhD) IRX001381 (PI Benjamin Hampstead, PhD); University of New Mexico - P20 AG068077 (Gary Rosenberg, MD); University of Pennsylvania - State of PA project 2019NF4100087335 (PI David Wolk, MD); Rooney Family Research Fund (PI David Wolk, MD); R01 AG055005 (PI David Wolk, MD); University of Pittsburgh - P50 AG005133 (PI Oscar Lopez MD); University of Southern California - P50 AG005142 (PI Helena Chui MD); University of

Washington - P50 AG005136 (PI Thomas Grabowski MD); University of Wisconsin - P50 AG033514 (PI Sanjay Asthana MD FRCP); Vanderbilt University – P20 AG068082; Wake Forest - P30AG072947 (PI Suzanne Craft, PhD); Washington University, St. Louis - P01 AG03991 (PI John Morris MD); P01 AG026276 (PI John Morris MD); P20 MH071616 (PI Dan Marcus); P30 AG066444 (PI John Morris MD); P30 NS098577 (PI Dan Marcus); R01 AG021910 (PI Randy Buckner); R01 AG043434 (PI Catherine Roe); R01 EB009352 (PI Dan Marcus); UL1 TR000448 (PI Brad Evanoff); U24 RR021382 (PI Bruce Rosen); Avid Radiopharmaceuticals / Eli Lilly; Yale - P50 AG047270 (PI Stephen Strittmatter MD PhD); R01AG052560 (MPI: Christopher van Dyck, MD; Richard Carson, PhD); R01AG062276 (PI: Christopher van Dyck, MD); 1Florida - P30AG066506-03 (PI Glenn Smith, PhD); P50 AG047266 (PI Todd Golde MD PhD)

Competing Interests

The authors report no competing interests.

Supplementary Material

Supplementary figures and tables available online.

Appendix 1

Group/Consortium Authors

A) HABS-HD MPIs: Sid E O'Bryant, Kristine Yaffe, Arthur Toga, Robert Rissman, & Leigh Johnson; and the HABS-HD Investigators: Meredith Braskie, Kevin King, James R Hall, Melissa Petersen, Raymond Palmer, Robert Barber, Yonggang Shi, Fan Zhang, Rajesh Nandy, Roderick McColl, David Mason, Bradley Christian, Nicole Phillips, Stephanie Large, Joe Lee, Badri Vardarajan, Monica Rivera Mindt, Amrita Cheema, Lisa Barnes, Mark Mapstone, Annie Cohen, Amy Kind, Ozioma Okonkwo, Raul Vintimilla, Zhengyang Zhou, Michael Donohue, Rema Raman, Matthew Borzage, Michelle Mielke, Beau Ances, Ganesh Babulal, Jorge Llibre-Guerra, Carl Hill and Rocky Vig.

B) Data used in preparation of this article were obtained from the Alzheimer's Disease Neuroimaging Initiative (ADNI) database (adni.loni.usc.edu). As such, the investigators within the ADNI contributed to the design and implementation of ADNI and/or provided data but did not participate in analysis or writing of this report. A complete listing of ADNI investigators can be found at: http://adni.loni.usc.edu/wp-content/uploads/how_to_apply/ADNI_Acknowledgement_List.pdf

C) Data used in preparation of this article were derived from BIOCARD study, supported by grant U19 – AG033655 from the National Institute on Aging. The BIOCARD study team did not participate in the analysis or writing of this report, however, they contributed to the design and implementation of the study. A listing of BIOCARD investigators can be found on the BIOCARD website (on the 'BIOCARD Data Access Procedures' page, 'Acknowledgement Agreement' document).

References

1. Ocklenburg S, Mundorf A, Gerrits R, Karlsson EM, Papadatou-Pastou M, Vingerhoets G. Clinical implications of brain asymmetries. *Nat Rev Neurol*. Jul 2024;20(7):383-394. doi:10.1038/s41582-024-00974-8

2. Dax M. Lesions de la motie gauche de l'encephale coincident avec l'oublie des signes de la pensee. *Gaz Hbd Med Chir*. 1865;2:259-262.

3. Manning L, Thomas-Anterion C. Marc Dax and the discovery of the lateralisation of language in the left cerebral hemisphere. *Rev Neurol (Paris)*. Dec 2011;167(12):868-72. doi:10.1016/j.neurol.2010.10.017

4. Broca P. Perte de la parole, ramollissement chronique et destruction partielle du lobe antérieur gauche du cerveau. *Bull Soc Anthropol*. 1861;2(1):235-238.

5. Amunts K, Schleicher A, Burgel U, Mohlberg H, Uylings HB, Zilles K. Broca's region revisited: cytoarchitecture and intersubject variability. *J Comp Neurol*. Sep 20 1999;412(2):319-41. doi:10.1002/(sici)1096-9861(19990920)412:2<319::aid-cne10>3.0.co;2-7

6. Brincat SL, Miller EK. Cognitive independence and interactions between cerebral hemispheres. *Neuropsychologia*. Jun 6 2025;212:109153. doi:10.1016/j.neuropsychologia.2025.109153

7. Bishop DV. Cerebral asymmetry and language development: cause, correlate, or consequence? *Science*. Jun 14 2013;340(6138):1230531. doi:10.1126/science.1230531

8. Thiebaut de Schotten M, Dell'Acqua F, Forkel SJ*, et al*. A lateralized brain network for visuospatial attention. *Nat Neurosci*. Sep 18 2011;14(10):1245-6. doi:10.1038/nn.2905

9. Callaert DV, Vercauteren K, Peeters R*, et al*. Hemispheric asymmetries of motor versus nonmotor processes during (visuo)motor control. *Hum Brain Mapp*. Aug 2011;32(8):1311-29. doi:10.1002/hbm.21110

10. Forkel SJ, Friedrich P, Thiebaut de Schotten M, Howells H. White matter variability, cognition, and disorders: a systematic review. *Brain Struct Funct*. Mar 2022;227(2):529-544. doi:10.1007/s00429-021-02382-w

11. Sporns O, Tononi G, Kotter R. The human connectome: A structural description of the human brain. *PLoS Comput Biol*. Sep 2005;1(4):e42. doi:10.1371/journal.pcbi.0010042

12. Biswal BB, Mennes M, Zuo XN*, et al*. Toward discovery science of human brain function. *Proc Natl Acad Sci U S A*. Mar 9 2010;107(10):4734-9. doi:10.1073/pnas.0911855107

13. Jeurissen B, Descoteaux M, Mori S, Leemans A. Diffusion MRI fiber tractography of the brain. *NMR Biomed*. 04 2019;32(4):e3785. doi:10.1002/nbm.3785

14. Alexander DC, Dyrby TB, Nilsson M, Zhang H. Imaging brain microstructure with diffusion MRI: practicality and applications. *NMR Biomed*. 04 2019;32(4):e3841. doi:10.1002/nbm.3841

15. Yeh FC. Shape analysis of the human association pathways. *Neuroimage*. Dec 2020;223:117329. doi:10.1016/j.neuroimage.2020.117329

16. Beaulieu C. The basis of anisotropic water diffusion in the nervous system - a technical review. *NMR Biomed*. 2002 Nov-Dec 2002;15(7-8):435-55. doi:10.1002/nbm.782

17. Takao H, Hayashi N, Ohtomo K. White matter microstructure asymmetry: effects of volume asymmetry on fractional anisotropy asymmetry. *Neuroscience*. Feb 12 2013;231:1-12. doi:10.1016/j.neuroscience.2012.11.038

18. Shu N, Liu Y, Duan Y, Li K. Hemispheric Asymmetry of Human Brain Anatomical Network Revealed by Diffusion Tensor Tractography. *Biomed Res Int*. 2015;2015:908917. doi:10.1155/2015/908917

19. Carper RA, Treiber JM, DeJesus SY, Müller RA. Reduced Hemispheric Asymmetry of White Matter Microstructure in Autism Spectrum Disorder. *J Am Acad Child Adolesc Psychiatry*. Dec 2016;55(12):1073-1080. doi:10.1016/j.jaac.2016.09.491

20. Hau J, Sarubbo S, Houde JC*, et al*. Revisiting the human uncinate fasciculus, its subcomponents and asymmetries with stem-based tractography and microdissection validation. *Brain Struct Funct*. May 2017;222(4):1645-1662. doi:10.1007/s00429-016-1298-6

21. Honnedevasthana Arun A, Connelly A, Smith RE, Calamante F. Characterisation of white matter asymmetries in the healthy human brain using diffusion MRI fixel-based analysis. *Neuroimage*. Jan 15 2021;225:117505. doi:10.1016/j.neuroimage.2020.117505

22. Demnitz N, Madsen KS, Johnsen LK, Kjaer M, Boraxbekk CJ, Siebner HR. Right-left asymmetry in corticospinal tract microstructure and dexterity are uncoupled in late adulthood. *Neuroimage*. Oct 15 2021;240:118405. doi:10.1016/j.neuroimage.2021.118405

23. Shu M, Yu C, Shi Q*, et al*. Alterations in white matter integrity and asymmetry in patients with benign childhood epilepsy with centrotemporal spikes and childhood absence epilepsy: An automated fiber quantification tractography study. *Epilepsy Behav*. Oct 2021;123:108235. doi:10.1016/j.yebeh.2021.108235

24. Mundorf A, Peterburs J, Ocklenburg S. Asymmetry in the Central Nervous System: A Clinical Neuroscience Perspective. *Front Syst Neurosci*. 2021;15:733898. doi:10.3389/fnsys.2021.733898

25. Roe JM, Vidal-Pineiro D, Amlien IK*, et al*. Tracing the development and lifespan change of population-level structural asymmetry in the cerebral cortex. *Elife*. Jun 19 2023;12doi:10.7554/eLife.84685

26. Kumpulainen V, Merisaari H, Silver E*, et al*. Sex differences, asymmetry, and age-related white matter development in infants and 5-year-olds as assessed with tract-based spatial statistics. *Hum Brain Mapp*. May 2023;44(7):2712-2725. doi:10.1002/hbm.26238

27. Zhu Y, Li S, Da X*, et al*. Study of the relationship between onset lateralization and hemispheric white matter asymmetry in Parkinson's disease. *J Neurol*. Oct 2023;270(10):5004-5016. doi:10.1007/s00415-023-11849-1

28. Cai LY, Yang Q, Hansen CB*, et al*. PreQual: An automated pipeline for integrated preprocessing and quality assurance of diffusion weighted MRI images. *Magn Reson Med*. Jul 2021;86(1):456-470. doi:10.1002/mrm.28678

29. Kim ME, Gao C, Ramadass K, *et al*. Scalable quality control on processing of large diffusion-weighted and structural magnetic resonance imaging datasets. *arXiv preprint arXiv:240917286*. 2024;

30. Kim ME, Ramadass K, Gao C, *et al*. Scalable, reproducible, and cost-effective processing of large-scale medical imaging datasets. *arXiv preprint arXiv:240814611*. 2024;

31. Wasserthal J, Neher P, Maier-Hein KH. TractSeg - Fast and accurate white matter tract segmentation. *Neuroimage*. Dec 2018;183:239-253. doi:10.1016/j.neuroimage.2018.07.070

32. scilus/scilpy. The sherbrooke connectivity imaging lab (scil) python dmri processing tool- box.

33. Wheeler-Kingshott CA, Cercignani M. About "axial" and "radial" diffusivities. *Magn Reson Med*. May 2009;61(5):1255-60. doi:10.1002/mrm.21965

34. Schilling KG, Chad JA, Chamberland M, *et al*. White matter tract microstructure, macrostructure, and associated cortical gray matter morphology across the lifespan. *Imaging Neuroscience*. 2023;1:1-24. doi:10.1162/imag_a_00050

35. Savic I, Lindström P. PET and MRI show differences in cerebral asymmetry and functional connectivity between homo- and heterosexual subjects. *Proc Natl Acad Sci U S A*. Jul 08 2008;105(27):9403-8. doi:10.1073/pnas.0801566105

36. Grummer-Strawn LM, Reinold C, Krebs NF, Centers for Disease C, Prevention. Use of World Health Organization and CDC growth charts for children aged 0-59 months in the United States. *MMWR Recomm Rep*. Sep 10 2010;59(RR-9):1-15.

37. Santoni G, Calderon-Larranaga A, Vetrano DL, Welmer AK, Orsini N, Fratiglioni L. Geriatric Health Charts for Individual Assessment and Prediction of Care Needs: A Population-Based Prospective Study. *J Gerontol A Biol Sci Med Sci*. Jan 1 2020;75(1):131-138. doi:10.1093/gerona/gly272

38. Bethlehem RAI, Seidlitz J, White SR, *et al*. Brain charts for the human lifespan. *Nature*. Apr 2022;604(7906):525-533. doi:10.1038/s41586-022-04554-y

39. Rigby RA, Stasinopoulos DM. Generalized Additive Models for Location, Scale and Shape. *Journal of the Royal Statistical Society Series C: Applied Statistics*. 2005;54(3):507-554. doi:10.1111/j.1467-9876.2005.00510.x

40. Bethlehem RAI, Seidlitz J, White SR, *et al*. Brain charts for the human lifespan. *Nature*. Apr 2022;604(7906):525-533. doi:10.1038/s41586-022-04554-y

41. Dubois J, Grotheer M, Yang JY, Tournier JD, Beaulieu C, Lebel C. Small brains but big challenges: white matter tractography in early life samples. *Brain Struct Funct*. Apr 28 2025;230(4):58. doi:10.1007/s00429-025-02922-8

42. Dubois J, Dehaene-Lambertz G, Kulikova S, Poupon C, Huppi PS, Hertz-Pannier L. The early development of brain white matter: a review of imaging studies in fetuses, newborns and infants. *Neuroscience*. Sep 12 2014;276:48-71. doi:10.1016/j.neuroscience.2013.12.044

43. Habeck C, Razlighi Q, Gazes Y, Barulli D, Steffener J, Stern Y. Cognitive Reserve and Brain Maintenance: Orthogonal Concepts in Theory and Practice. *Cereb Cortex*. Aug 1 2017;27(8):3962-3969. doi:10.1093/cercor/bhw208

44. Dulyan L, Bortolami C, Forkel SJ. Chapter 2 - Asymmetries in the human brain. In: Papagno C, Corballis P, eds. *Handbook of Clinical Neurology*. Elsevier; 2025:15-36.

45. Parekh SA, Wren-Jarvis J, Lazerwitz M*, et al*. Hemispheric lateralization of white matter microstructure in children and its potential role in sensory processing dysfunction. *Front Neurosci*. 2023;17:1088052. doi:10.3389/fnins.2023.1088052

46. Angstmann S, Madsen KS, Skimminge A, Jernigan TL, Baaré WF, Siebner HR. Microstructural asymmetry of the corticospinal tracts predicts right-left differences in circle drawing skill in right-handed adolescents. *Brain Struct Funct*. Dec 2016;221(9):4475-4489. doi:10.1007/s00429-015-1178-5

47. Schmithorst VJ, Holland SK, Dardzinski BJ. Developmental differences in white matter architecture between boys and girls. *Hum Brain Mapp*. Jun 2008;29(6):696-710. doi:10.1002/hbm.20431

48. Schilling KG, Rheault F, Petit L*, et al*. Tractography dissection variability: What happens when 42 groups dissect 14 white matter bundles on the same dataset? *Neuroimage*. Aug 22 2021;243:118502. doi:10.1016/j.neuroimage.2021.118502

49. Kim ME, Gao C, Ramadass K*, et al*. White matter microstructure and macrostructure brain charts across the human lifespan. *bioRxiv*. 2025:2025.05.08.652953. doi:10.1101/2025.05.08.652953

50. Thiebaut de Schotten M, Ffytche DH, Bizzi A*, et al*. Atlasing location, asymmetry and inter-subject variability of white matter tracts in the human brain with MR diffusion tractography. *Neuroimage*. Jan 1 2011;54(1):49-59. doi:10.1016/j.neuroimage.2010.07.055

51. Ocklenburg S, Friedrich P, Güntürkün O, Genç E. Voxel-wise grey matter asymmetry analysis in left- and right-handers. *Neurosci Lett*. Oct 28 2016;633:210-214. doi:10.1016/j.neulet.2016.09.046

52. Good CD, Johnsrude I, Ashburner J, Henson RN, Friston KJ, Frackowiak RS. Cerebral asymmetry and the effects of sex and handedness on brain structure: a voxel-based morphometric analysis of 465 normal adult human brains. *Neuroimage*. Sep 2001;14(3):685-700. doi:10.1006/nimg.2001.0857

53. Minkova L, Habich A, Peter J, Kaller CP, Eickhoff SB, Klöppel S. Gray matter asymmetries in aging and neurodegeneration: A review and meta-analysis. *Hum Brain Mapp*. Dec 2017;38(12):5890-5904. doi:10.1002/hbm.23772

54. Toga AW, Thompson PM. Mapping brain asymmetry. *Nat Rev Neurosci*. Jan 2003;4(1):37-48. doi:10.1038/nrn1009

55. Ford A, Ammar Z, Li L, Shultz S. Lateralization of major white matter tracts during infancy is time-varying and tract-specific. *Cereb Cortex*. Sep 26 2023;33(19):10221-10233. doi:10.1093/cercor/bhad277

56. Kumpulainen V. *Brain white matter development, associations to maternal perinatal psychological distress and emotional attention at the age of 5 years*. fi=Turun yliopisto|en=University of Turku; 2024.

57. Lebel C, Treit S, Beaulieu C. A review of diffusion MRI of typical white matter development from early childhood to young adulthood. *NMR Biomed*. Apr 2019;32(4):e3778. doi:10.1002/nbm.3778

58. Dubois J, Poupon C, Thirion B, *et al*. Exploring the Early Organization and Maturation of Linguistic Pathways in the Human Infant Brain. *Cereb Cortex*. May 2016;26(5):2283-98. doi:10.1093/cercor/bhv082

59. Miyata J, Sasamoto A, Koelkebeck K, *et al*. Abnormal asymmetry of white matter integrity in schizophrenia revealed by voxelwise diffusion tensor imaging. *Hum Brain Mapp*. Jul 2012;33(7):1741-9. doi:10.1002/hbm.21326

60. Joseph RM, Fricker Z, Fenoglio A, Lindgren KA, Knaus TA, Tager-Flusberg H. Structural asymmetries of language-related gray and white matter and their relationship to language function in young children with ASD. *Brain Imaging Behav*. Mar 2014;8(1):60-72. doi:10.1007/s11682-013-9245-0

61. Claassen DO, McDonell KE, Donahue M, *et al*. Cortical asymmetry in Parkinson's disease: early susceptibility of the left hemisphere. *Brain Behav*. Dec 2016;6(12):e00573. doi:10.1002/brb3.573

62. Catani M, Craig MC, Forkel SJ, *et al*. Altered integrity of perisylvian language pathways in schizophrenia: relationship to auditory hallucinations. *Biol Psychiatry*. Dec 15 2011;70(12):1143-50. doi:10.1016/j.biopsych.2011.06.013

63. Amemiya K, Naito E, Takemura H. Age dependency and lateralization in the three branches of the human superior longitudinal fasciculus. *Cortex*. Jun 2021;139:116-133. doi:10.1016/j.cortex.2021.02.027

64. Barrick TR, Lawes IN, Mackay CE, Clark CA. White matter pathway asymmetry underlies functional lateralization. *Cereb Cortex*. Mar 2007;17(3):591-8. doi:10.1093/cercor/bhk004

65. Baudo MC, Colombo EE, Pérez MA, *et al*. Three-Dimensional Anatomy of the Anterior Commissure: A Tractography and Anatomical Study. *World Neurosurg*. Mar 2022;159:e365-e374. doi:10.1016/j.wneu.2021.12.059

66. Briggs RG, Khan AB, Chakraborty AR, *et al*. Anatomy and White Matter Connections of the Superior Frontal Gyrus. *Clin Anat*. Sep 2020;33(6):823-832. doi:10.1002/ca.23523

67. Buchel C, Raedler T, Sommer M, Sach M, Weiller C, Koch MA. White matter asymmetry in the human brain: a diffusion tensor MRI study. *Cereb Cortex*. Sep 2004;14(9):945-51. doi:10.1093/cercor/bhh055

68. Budisavljevic S, Castiello U, Begliomini C. Handedness and White Matter Networks. *Neuroscientist*. Feb 2021;27(1):88-103. doi:10.1177/1073858420937657

69. Catani M, Allin MP, Husain M, *et al*. Symmetries in human brain language pathways correlate with verbal recall. *Proc Natl Acad Sci U S A*. Oct 23 2007;104(43):17163-8. doi:10.1073/pnas.0702116104

70. Dalamagkas K, Tsintou M, Rathi Y, *et al*. Individual variations of the human corticospinal tract and its hand-related motor fibers using diffusion MRI tractography. *Brain Imaging Behav*. Jun 2020;14(3):696-714. doi:10.1007/s11682-018-0006-y

71. Dayan M, Munoz M, Jentschke S, *et al*. Optic radiation structure and anatomy in the normally developing brain determined using diffusion MRI and tractography. *Brain Struct Funct*. Jan 2015;220(1):291-306. doi:10.1007/s00429-013-0655-y

72. Glasser MF, Rilling JK. DTI tractography of the human brain's language pathways. *Cereb Cortex*. Nov 2008;18(11):2471-82. doi:10.1093/cercor/bhn011

73. Gong G, Jiang T, Zhu C*, et al*. Asymmetry analysis of cingulum based on scale-invariant parameterization by diffusion tensor imaging. *Hum Brain Mapp*. Feb 2005;24(2):92-8. doi:10.1002/hbm.20072

74. Hasan KM, Iftikhar A, Kamali A*, et al*. Development and aging of the healthy human brain uncinate fasciculus across the lifespan using diffusion tensor tractography. *Brain Res*. Jun 18 2009;1276:67-76. doi:10.1016/j.brainres.2009.04.025

75. Lebel C, Beaulieu C. Lateralization of the arcuate fasciculus from childhood to adulthood and its relation to cognitive abilities in children. *Hum Brain Mapp*. Nov 2009;30(11):3563-73. doi:10.1002/hbm.20779

76. Panesar SS, Belo JTA, Yeh FC, Fernandez-Miranda JC. Structure, asymmetry, and connectivity of the human temporo-parietal aslant and vertical occipital fasciculi. *Brain Struct Funct*. Mar 2019;224(2):907-923. doi:10.1007/s00429-018-1812-0

77. Powell HW, Parker GJ, Alexander DC*, et al*. Hemispheric asymmetries in language-related pathways: a combined functional MRI and tractography study. *Neuroimage*. Aug 01 2006;32(1):388-99. doi:10.1016/j.neuroimage.2006.03.011

78. Putnam MC, Steven MS, Doron KW, Riggall AC, Gazzaniga MS. Cortical projection topography of the human splenium: hemispheric asymmetry and individual differences. *J Cogn Neurosci*. Aug 2010;22(8):1662-9. doi:10.1162/jocn.2009.21290

79. Sboto-Frankenstein UN, Lazar T, Bolster RB*, et al*. Symmetry of the fornix using diffusion tensor imaging. *J Magn Reson Imaging*. Oct 2014;40(4):929-36. doi:10.1002/jmri.24424

80. Silk TJ, Vilgis V, Adamson C*, et al*. Abnormal asymmetry in frontostriatal white matter in children with attention deficit hyperactivity disorder. *Brain Imaging and Behavior*. 2016/12/01 2016;10(4):1080-1089. doi:10.1007/s11682-015-9470-9

81. Vernooij MW, Smits M, Wielopolski PA, Houston GC, Krestin GP, van der Lugt A. Fiber density asymmetry of the arcuate fasciculus in relation to functional hemispheric language lateralization in both right- and left-handed healthy subjects: a combined fMRI and DTI study. *Neuroimage*. Apr 15 2007;35(3):1064-76. doi:10.1016/j.neuroimage.2006.12.041

82. Wilde EA, McCauley SR, Chu Z*, et al*. Diffusion tensor imaging of hemispheric asymmetries in the developing brain. *J Clin Exp Neuropsychol*. Feb 2009;31(2):205-18. doi:10.1080/13803390802098118

83. Wu Y, Sun D, Wang Y. Subcomponents and Connectivity of the Inferior Fronto-Occipital Fasciculus Revealed by Diffusion Spectrum Imaging Fiber Tracking. *Front Neuroanat*. 2016;10:88. doi:10.3389/fnana.2016.00088